TWO-DIMENSIONAL WIND-TUNNEL TEST ON A VARIABLE -CAMBER AIRFOIL WITH DISTRIBUTED SUCTION BOUNDARY-LAYER CONTROL

L. J. Mertaugh, et al

Mississippi State University

Prepared for:

Army Air Mobility Research and Development Laboratory

May 1973

AD

USAAMRDL TECHNICAL REPORT 73-3

TWO-DIMENSIONAL WIND-TUNNEL TEST ON A VARIABLE-CAMBER AIRFOIL WITH DISTRIBUTED SUCTION BOUNDARY-LAYER CONTROL

By

L. J. Mertaugh
N. S. Kiran
S. Dey

May 1973

EUSTIS DIRECTORATE
U. S. ARMY AIR MOBILITY RESEARCH AND DEVELOPMENT LABORATORY
FORT EUSTIS, VIRGINIA

CONTRACT DAAJ02-67-C-0016
THE DEPARTMENT OF AEROPHYSICS AND AEROSPACE ENGINEERING
MISSISSIPPI STATE UNIVERSITY
STATE COLLEGE, MISSISSIPPI

72

DISCLAIMERS

The findings in this report are not to be construed as an official Department of the Army position unless so designated by other authorized documents.

When Government drawings, specifications, or other data are used for any purpose other than in connection with a definitely related Government procurement operation, the U. S. Government thereby incurs no responsibility nor any obligation whatsoever; and the fact that the Government may have formulated, furnished, or in any way supplied the said drawings, specifications, or other data is not to be regarded by implication or otherwise as in any manner licensing the holder or any other person or corporation, or conveying any rights or permission, to manufacture, use, or sell any patented invention that may in any way be related thereto.

Trade names cited in this report do not constitute an official endorsement or approval of the use of such commercial hardware or software.

DISPOSITION INSTRUCTIONS

Destroy this report when no longer needed. Do not return it to the originator.

UNCLASSIFIED
Security Classification

DOCUMENT CONTROL DATA - R & D

(Security classification of title, body of abstract and indexing annotation must be entered when the overall report is classified)

1. ORIGINATING ACTIVITY (Corporate author) Mississippi State University Department of Aerophysics & Aerospace Engineering State College, Mississippi	2a. REPORT SECURITY CLASSIFICATION UNCLASSIFIED 2b. GROUP

3. REPORT TITLE

TWO-DIMENSIONAL WIND-TUNNEL TEST ON A VARIABLE-CAMBER AIRFOIL WITH DISTRIBUTED SUCTION BOUNDARY-LAYER CONTROL

4. DESCRIPTIVE NOTES (Type of report and inclusive dates)
Final Report

Details of illustrations in this document may be better studied on microfiche.

5. AUTHOR(S) (First name, middle initial, last name)

L. J. Mertaugh
N. S. Kiran
S. Dey

6. REPORT DATE	7a. TOTAL NO. OF PAGES	7b. NO. OF REFS
May 1973	72	14

8a. CONTRACT OR GRANT NO.	9a. ORIGINATOR'S REPORT NUMBER(S)
DAAJ02-67-C-0016 b. PROJECT NO. Task 1F162204A14234 c. d.	USAAMRDL Technical Report 73-3 9b. OTHER REPORT NO(S) (Any other numbers that may be assigned this report) EIRS-ASE-73-2

10. DISTRIBUTION STATEMENT

Approved for public release; distribution unlimited.

11. SUPPLEMENTARY NOTES	12. SPONSORING MILITARY ACTIVITY
	Eustis Directorate U. S. Army Air Mobility R & D Laboratory Fort Eustis, Virginia

13. ABSTRACT

This report presents the results of a test program that was intended to (1) investigate possible improvements in the methods used to predict the suction distribution required to prevent separation of the turbulent boundary layer at high lift coefficients and (2) provide experimental data on a variable-camber airfoil with distributed-suction boundary-layer control. The theoretical method used to predict the required suction distribution utilized the momentum and energy integral equations with various empirical relationships for the boundary-layer variables. A constant value of H_{12} was assumed in these calculations. Two, 2-dimensional wind-tunnel models were tested. One model incorporated the variable-camber feature and was tested, without boundary-layer control, at 0°, 5°, and 10° of camber. The second model was of the 30°-camber configuration and had a distributed-suction boundary-layer control system. The suction was provided through rows of closely spaced holes. The dimensions of both models were consistent with a 16-inch, 0°-camber chord line. Test speeds between 56 and 131 feet per second were used. Model lift and moment data were obtained. The maximum lift coefficient for the 30°-camber configuration was 3.6. The theoretical suction-velocity distribution did not allow the design lift coefficient to be developed. The failure of the theoretical method is felt to be due to inadequacies in the empirical relationship used to determine the wall shear stress as a function of suction velocity.

DD FORM 1 NOV 68 1473 REPLACES DD FORM 1473, 1 JAN 64, WHICH IS OBSOLETE FOR ARMY USE.

UNCLASSIFIED
Security Classification

UNCLASSIFIED

Security Classification

14 KEY WORDS	LINK A		LINK B		LINK C	
	ROLE	WT	ROLE	WT	ROLE	WT
High Lift						
Boundary Layer Control						
Turbulent Boundary Layer						
2-D wind tunnel test						
Variable camber						

UNCLASSIFIED

Security Classification

5742-73

DEPARTMENT OF THE ARMY
U. S. ARMY AIR MOBILITY RESEARCH & DEVELOPMENT LABORATORY
EUSTIS DIRECTORATE
FORT EUSTIS, VIRGINIA 23604

This report has been reviewed by the U. S. Army Air Mobility Research and Development Laboratory, and is considered to be technically sound. The report is published for the exchange of information and the stimulation of ideas. The program was conducted under the technical management of Mr. Frederick A. Raitch of the Technology Applications Division of this Directorate.

Task 1F162204A14234
Contract DAAJ02-67-C-0016
USAAMRDL Technical Report 73-3
May 1973

TWO-DIMENSIONAL WIND-TUNNEL TEST ON A VARIABLE-CAMBER AIRFOIL WITH DISTRIBUTED SUCTION BOUNDARY-LAYER CONTROL

EIRS-ASE-73-2

By

L. J. Mertaugh
N. S. Kiran
S. Dey

Prepared by
Mississippi State University
Engineering and Industrial Research Station
Department of Aerophysics and Aerospace Engineering
State College, Mississippi

for

EUSTIS DIRECTORATE
U. S. ARMY AIR MOBILITY RESEARCH AND DEVELOPMENT LABORATORY
FORT EUSTIS, VIRGINIA

ABSTRACT

This report presents the results of a test program that was intended to (1) investigate possible improvements in the methods used to predict the suction distribution required to prevent separation of the turbulent boundary layer at high lift coefficients and (2) provide experimental data on a variable-camber airfoil with distributed-suction boundary-layer control. The theoretical method used to predict the required suction distribution utilized the momentum and energy integral equations with various empirical relationships for the boundary-layer variables. A constant value of H_{12} was assumed in these calculations. Two, 2-dimensional wind-tunnel models were tested. One model incorporated the variable-camber feature and was tested, without boundary-layer control, at 0°, 5°, and 10° of camber. The second model was of the 30°-camber configuration and had a distributed-suction boundary-layer control system. The suction was provided through rows of closely spaced holes. The dimensions of both models were consistent with a 16-inch, 0°-camber chord line. Test speeds between 56 and 131 feet per second were used. Model lift and moment data were obtained. The maximum lift coefficient for the 30°-camber configuration was 3.6. The theoretical suction-velocity distribution did not allow the design lift coefficient to be developed. The failure of the theoretical method is felt to be due to inadequacies in the empirical relationship used to determine the wall shear stress as a function of suction velocity.

TABLE OF CONTENTS

LIST OF ILLUSTRATIONS

LIST OF SYMBOLS

A	shear stress constant
B	energy dissipation constant
C	momentum integral equation constant
C_l	section lift coefficient
$C_{m_{l.e.}}$	section moment coefficient with respect to the airfoil leading edge
C_p	pressure coefficient
c	chord length, ft
D	momentum thickness equation constant, $(ft^2/sec)^{0.268}$
d	suction hole diameter, in.
d_l	energy dissipation function, lb/ft-sec
H_{12}	first boundary-layer shape parameter ($H_{12} = \delta_1/\delta_2$)
H_{32}	second boundary-layer shape parameter ($H_{32} = \delta_3/\delta_2$)
l.e.	leading edge
p	static pressure, lb/ft^2 or in. H_2O
P_{i_1}	leading-edge suction plenum pressure, lb/ft^2 or in. of H_2O
P_{i_2}	aft suction plenum pressure, lb/ft^2 or in. of H_2O
Δp	differential pressure across the suction holes, lb/ft^2 or in. of H_2O
Q	suction volume rate of flow, ft^3/min
R_N	Reynolds number based on chord length and free-stream velocity
$R_{\delta 2}$	Reynolds number based on the boundary-layer momentum thickness and the local velocity

S	surface distance measured from the leading edge of the airfoil, ft or in.
S_t	total surface distance (16.73 in.), ft or in.
t_1	turbulent energy function, lb/ft-sec
U	local velocity outside the boundary layer, ft/sec
U_∞	free-stream velocity, ft/sec
v_s	suction velocity (positive into the surface), ft/sec
x	distance measured along the chord line, ft or in.
α	angle of attack, deg
δ_1	boundary-layer displacement thickness, ft or in.
δ_2	boundary-layer momentum thickness, ft or in.
δ_3	boundary-layer energy thickness, ft or in.
ν	coefficient of kinematic viscosity, ft^2/sec
ρ	density, $slugs/ft^3$
τ_w	wall shear stress, lb/ft^2

SUBSCRIPTS

o	initial conditions
std	standard sea-level conditions
∞	free-stream conditions

INTRODUCTION

The use of distributed-suction boundary-layer control for providing high lift coefficients on STOL aircraft has been studied at Mississippi State University for a number of years. A number of test vehicles have been utilized to investigate various aspects of this area of research, and at the present time this facility has two aircraft flying with functional, high-lift, distributed-suction boundary-layer control systems. The first aircraft is a modified L-19 and has demonstrated trimmed lift coefficients of 4.8; see Reference 1. The second aircraft is the XV-11A (see Reference 2) which incorporates a unique, variable-camber wing configuration as well as the distributed-suction boundary-layer control system. The variable wing camber is intended to allow more efficient utilization of the boundary-layer control system while avoiding the protuberances and surface discontinuities normally associated with mechanical high-lift devices. The XV-11A has provided trimmed lift coefficients of 2.7; the boundary-layer control system, however, is not considered to be optimum and its full potential has not been realized.

Throughout all of these studies of the use of distributed-suction, high-lift boundary-layer control, the lack of theoretical methods for correctly predicting the required suction distribution has been evident. The successful suction configurations have all resulted from extensive trial-and-error experimentation. Efforts to analyze the successful suction configurations have been limited, with only marginal results being obtained. In the case of the XV-11A aircraft, this difficulty is compounded by the lack of wind-tunnel test data on the variable-camber airfoil section.

The present research program was intended to investigate possible improvements in the methods used to predict the required suction distribution and to provide experimental verification of the computed results as well as basic force and moment data on the XV-11A airfoil section.

The prediction of the required suction distribution was based on the momentum and energy integral equations. Modifications to empirical relations for the shear-stress and energy-dissipation terms were used to account for the effect of suction. Additional calculations, using the method of R. Eppler, were performed to provide an alternate suction distribution.

The wind-tunnel test program used two, 2-dimensional airfoil section models which had a span and an actual, or equivalent, 0°-camber chord of 16 inches. The models were tested in the low-speed, closed-circuit wind tunnel at Mississippi State University. False walls were installed in the tunnel to give a two-dimensional test section of 1.33 x 4 feet. One model incorporated the variable-camber configuration and was not provided with

boundary-layer control. This variable-camber model was tested in the 0°-, 5°-, and 10°-camber configurations. The suction model was constructed in the 30°-camber configuration with suction provided through closely spaced rows of suction holes drilled in the upper surface of the model. The final suction configuration consisted of 142 rows of suction holes. The first 4 rows of suction holes were located near the leading edge of the model. The remaining 138 rows of suction holes extended from approximately 19 percent of the chord to the trailing edge. The diameters of the suction holes along the airfoil were 0.007, 0.010, 0.015 and 0.018 inch.

The average test Reynolds numbers, based on the 16-inch, 0°-camber chord, were 1.1×10^6 for the impervious model and 0.63×10^6 and 0.47×10^6 for the suction model. The corresponding free-stream velocities were nominally 131, 75, and 56 feet per second respectively. Total suction flow coefficients of up to 0.03, based on the 16-inch chord, were tested. Angles of attack through stall were tested.

TEST EQUIPMENT

WIND TUNNEL

The Mississippi State University low-speed wind tunnel was modified for this test program by the installation of false walls which provided the two-dimensional test section. The longitudinal position of the 7-foot-long walls was adjusted to provide uniform flow in the test section. Uniform flow was verified, prior to installing the model, through velocity measurements obtained from pressure rakes mounted at various locations within the test section. Two screens (0.011-inch, brass-wire, square-weave cloth) were installed in the settling chamber, upstream of the test section, to reduce the turbulence level in the test section. The final level of turbulence was found to be 0.4 percent, at the test velocities, when measured with a hot-wire anemometer. This turbulence level is equivalent to a turbulence factor of 1.33. Because the installation of the false walls made the data from the normal tunnel velocity system invalid, four sets of total-pressure probes and static-pressure taps were used to determine the velocity in the two-dimensional test section. Two of these sets were mounted on each false wall forward of the model. Suction flow was provided by a number of electrically driven centrifugal blowers. Blower speed was controlled with variable auto-transformers. Suction was used on the false walls, in the vicinity of the model, to reduce the spanwise flow variation over the model due to model-wall interference. The wall suction was adjusted during the test to give a constant spanwise loading on the model and to provide uniform spanwise boundary-layer characteristics as determined by tuft observations. The general test section configuration is shown in Figure 1.

MODELS

The two wind-tunnel models are shown in Figures 2 and 3. Wood and fiber-glass ribs and spars were used in both models, with 0.020-inch aluminum used for the skin. Bonded construction was utilized, and plastic filler was applied to insure true model contours. The model span and the 0°-camber chord were 16 inches. The suction-model chord was consistent with the 16-inch, 0°-camber chord. Hinged subspars were used with the variable-camber (impervious) model to allow for the "bending" of the aft portion of the model. Model camber was defined by the use of replaceable ribs installed at each end of the model. End ribs giving wing cambers of 0°, 5°, and 10° were used for this program. The surface ordinates of the impervious model, for 0°, 5°, and 10° camber, and the suction model, 30° camber, are given in Tables I and II. The ordinates are measured with respect to the 0°-camber chord line. The 0°-camber airfoil section was derived from the NACA 63_2-615 airfoil with the ordinates aft of the 35-percent chord

TABLE I. AIRFOIL COORDINATES, 0° and 5° CAMBER

0° CAMBER				5° CAMBER			
x_u (in.)	y_u (in.)	x_l (in.)	y_l (in.)	x_u (in.)	y_u (in.)	x_l (in.)	y_l (in.)
0.0	0.0	0.0	0.0	0.0	0.0	0.0	0.0
0.2	0.340	0.2	-0.280	0.2	0.340	0.2	-0.280
0.4	0.500	0.4	-0.390	0.4	0.500	0.4	-0.390
0.6	0.660	0.6	-0.455	0.6	0.660	0.6	-0.455
0.8	0.765	0.8	-0.505	0.8	0.765	0.8	-0.505
1.2	0.932	1.2	-0.547	1.2	0.932	1.2	-0.547
1.6	1.058	1.6	-0.587	1.6	1.058	1.6	-0.587
2.0	1.149	2.0	-0.590	2.0	1.149	2.0	-0.590
2.4	1.235	2.4	-0.678	2.4	1.235	2.4	-0.678
3.2	1.403	3.2	-0.751	3.2	1.403	3.2	-0.751
4.0	1.517	4.0	-0.815	4.0	1.517	4.0	-0.815
4.8	1.582	4.8	-0.819	4.8	1.582	4.8	-0.819
5.6	1.602	5.6	-0.815	5.6	1.602	5.6	-0.815
6.4	1.598	6.4	-0.798	6.355	1.554	6.410	-0.805
8.0	1.461	8.0	-0.691	7.975	1.435	8.001	-0.704
9.6	1.242	9.6	-0.465	9.543	1.159	9.581	-0.607
11.2	0.982	11.2	-0.285	11.219	0.790	11.196	-0.488
12.8	0.698	-	-	12.690	0.355	-	-
14.4	0.360	14.4	0.0	14.245	-0.120	14.180	-0.561
16.0	0.0	16.0	0.0	15.865	-0.610	15.865	-0.610
l.e. Radius = 0.375 in.				l.e. Radius = 0.375 in.			

TABLE II. AIRFOIL COORDINATES, 10° and 30° CAMBER

10° CAMBER				30° CAMBER			
x_u (in.)	y_u (in.)	x_l (in.)	y_l (in.)	x_u (in.)	y_u (in.)	x_l (in.)	y_l (in.)
0.0	0.0	0.0	0.0	0.0	0.0	0.0	0.0
0.2	0.340	0.2	-0.280	0.2	0.340	0.2	-0.280
0.4	0.500	0.4	-0.390	0.4	0.500	0.4	-0.390
0.6	0.660	0.6	-0.455	0.6	0.660	0.6	-0.455
0.8	0.765	0.8	-0.505	0.8	0.765	0.8	-0.505
1.2	0.932	1.2	-0.547	1.2	0.932	1.2	-0.547
1.6	1.058	1.6	-0.587	1.6	1.058	1.6	-0.587
2.0	1.149	2.0	-0.590	2.0	1.149	2.0	-0.590
2.4	1.235	2.4	-0.678	2.4	1.235	2.4	-0.678
3.2	1.403	3.2	-0.751	3.2	1.403	3.2	-0.751
4.0	1.517	4.0	-0.815	4.0	1.517	4.0	-0.815
4.8	1.582	4.8	-0.819	4.8	1.582	4.8	-0.819
5.6	1.602	5.6	-0.815	5.6	1.602	5.6	-0.815
6.395	1.519	6.430	-0.848	6.405	1.532	6.355	-0.830
8.045	1.385	7.981	-0.775	8.027	1.310	7.965	-0.820
9.630	1.062	9.600	-0.700	9.542	0.815	9.542	-0.946
11.218	0.606	11.208	-0.680	11.005	0.085	11.110	-1.270
12.656	0.066	-	-	12.275	-0.835	-	-
14.201	-0.550	14.131	-0.895	13.551	-1.851	13.400	-2.180
15.691	-1.178	15.691	-1.178	14.801	-2.920	14.801	-2.920
l.e. Radius = 0.375 in.				l.e. Radius = 0.375 in.			

line modified to raise the trailing edge by 2.1 percent of the chord length. The leading-edge radius on the tapered XV-11A wing was maintained at a constant value along the wing span. The wind-tunnel model was representative of the XV-11A wing airfoil section at a span station corresponding to the midspan of the variable-camber section of the wing. The models were mounted to the false walls of the tunnel by means of circular end plates. The model angle of attack was controlled by rotating the circular end plates within the corresponding circular cutouts in the false walls.

Pressure tap lines were routed out of the models through both end plates. Suction flow was removed from the suction model through flexible tubing which connected each end of the model to the appropriate blowers which were mounted outside the tunnel; see Figure 1. The leading-edge suction flow used an internal manifold which distributed the suction pressures along the span of the leading-edge plenum. One blower, mounted on the top of the tunnel, provided the leading-edge suction. Two blowers, one each on the top and bottom of the tunnel, were used for the aft suction. The aft ribs of the suction model were cut out to reduce suction-pressure losses, and the interior of the model, aft of the spar, was used as a single plenum.

Two chordwise and two spanwise rows of static-pressure taps were used on the impervious model. Thirty-seven taps were provided in each chordwise row. Fourteen pressure taps, in addition to the corresponding two taps in each chordwise row, were used in each spanwise row of pressure taps. One chordwise and two spanwise rows of pressure taps were used in the suction model. The reduced number of static pressure taps in the suction model was a result of space limitations within this model. Four internal pressure taps were used to measure the pressure in the model suction plenums. Internal pressure was also measured in the wall suction plenums.

The suction holes were drilled by hand in the suction-model skin. The definition of the final suction hole distribution is given in Table III. The lateral spacing of the suction holes in each row gave 10 holes per inch.

INSTRUMENTATION

Model force and moment data were obtained from model static-pressure data and wake rake data. The pressure data were measured by means of water manometers and a pressure transducer driving a digital voltmeter. The water manometer was used exclusively for the impervious model tests. The reduced test velocities used with the suction model made the accuracy of the water manometer questionable, and the pressure transducer was used to measure the model static-pressure and the tunnel velocity data for the suction model tests. The lower velocities used with the suction model were

TABLE III. MODEL SUCTION HOLE GEOMETRY

Row	$S_{l.e.}$ (in.)	x/c	Holes Per Inch	Hole Diameter (in.)
1	.234	.0062	15.0	.010
2	.310	.0093	12.0	.007
3	.410	.0141	8.0	.007
4	.560	.0218	2.0	.007
5	3.495	.1861	13.0	.018
6	3.575	.1906	12.0	.018
7	3.661	.1954	11.5	.018
8	3.748	.2002	11.5	.018
9	3.838	.2053	11.0	.018
10	3.930	.2105	10.5	.018
11	4.027	.2160	10.0	.018
12	4.127	.2216	10.0	.018
13	4.231	.2274	9.5	.018
14	4.321	.2325	13.0	.015
15	4.400	.2369	12.5	.015
16	4.480	.2414	12.5	.015
17	4.562	.2460	12.0	.015
18	4.646	.2507	12.0	.015
19	4.733	.2556	11.5	.015
20	4.820	.2605	11.5	.015
21	4.909	.2655	11.0	.015
22	4.999	.2706	11.0	.015
23	5.091	.2757	10.5	.015
24	5.185	.2809	10.5	.015
25	5.282	.2864	10.5	.015
26	5.379	.2918	10.0	.015
27	5.479	.2975	10.0	.015
28	5.580	.3031	10.0	.015
29	5.680	.3087	9.5	.015
30	5.782	.3145	9.5	.015
31	5.886	.3203	9.5	.015
32	5.991	.3262	9.5	.015
33	6.098	.3322	9.5	.015
34	6.205	.3382	9.5	.015
35	6.324	.3449	9.0	.015
36	6.374	.3477	9.0	.015
37	6.483	.3537	9.0	.015
38	6.592	.3599	9.0	.015
39	6.700	.3660	9.0	.015
40	6.809	.3720	9.0	.015
41	6.918	.3782	8.5	.015
42	7.035	.3847	8.5	.015
43	7.152	.3913	8.5	.015
44	7.273	.3981	8.5	.015
45	7.395	.4049	8.5	.015
46	7.512	.4114	8.5	.015
47	7.629	.4180	8.5	.015
48	7.746	.4245	8.5	.015
49	7.863	.4311	8.5	.015
50	7.980	.4377	8.5	.015

TABLE III - Continued

Row	$S_{l.e.}$ (in.)	x/c	Holes Per Inch	Hole Diameter (in.)
51	8.097	.4443	8.5	.015
52	8.214	.4508	8.5	.015
53	8.332	.4574	9.0	.015
54	8.449	.4639	9.0	.015
55	8.562	.4703	9.0	.015
56	8.676	.4766	9.0	.015
57	8.797	.4834	9.0	.015
58	8.907	.4896	9.0	.015
59	9.021	.4959	9.0	.015
60	9.133	.5022	9.0	.015
61	9.250	.5087	9.0	.015
62	9.354	.5146	9.0	.015
63	9.463	.5206	9.0	.015
64	9.571	.5268	9.0	.015
65	9.680	.5328	9.0	.015
66	9.787	.5389	9.0	.015
67	9.894	.5448	9.5	.015
68	10.000	.5508	9.5	.015
69	10.105	.5566	9.5	.015
70	10.212	.5626	9.5	.015
71	10.317	.5685	9.5	.015
72	10.423	.5744	9.5	.015
73	10.527	.5802	9.5	.015
74	10.631	.5861	9.5	.015
75	10.735	.5918	9.5	.015
76	10.838	.5976	10.0	.015
77	10.940	.6033	10.0	.015
78	11.041	.6089	10.0	.015
79	11.141	.6146	10.0	.015
80	11.241	.6201	10.0	.015
81	11.342	.6758	10.0	.015
82	11.441	.6314	10.0	.015
83	11.541	.6369	10.0	.015
84	11.640	.6424	10.0	.015
85	11.738	.6479	10.0	.015
86	11.837	.6535	10.5	.015
87	11.934	.6588	10.5	.015
88	12.031	.6643	10.5	.015
89	12.127	.6697	10.5	.015
90	12.223	.6750	10.5	.015
91	12.319	.6804	10.5	.015
92	12.412	.6856	10.5	.015
93	12.506	.6908	10.5	.015
94	12.600	.6960	10.5	.015
95	12.693	.7013	11.0	.015
96	12.785	.7064	11.0	.015
97	12.877	.7115	11.0	.015
98	12.969	.7167	11.0	.015
99	13.061	.7218	11.0	.015
100	13.153	.7270	11.0	.015

TABLE III - Continued

Row	$S_{l.e.}$ (in.)	x/c	Holes Per Inch	Hole Diameter (in.)
101	13.245	.7321	11.0	.015
102	13.337	.7372	11.0	.015
103	13.427	.7423	11.0	.015
104	13.516	.7472	11.0	.015
105	13.606	.7522	11.0	.015
106	13.695	.7572	11.0	.015
107	13.783	.7621	11.5	.015
108	13.872	.7670	11.5	.015
109	13.961	.7720	11.5	.015
110	14.048	.7768	11.5	.015
111	14.135	.7818	11.5	.015
112	14.222	.7866	11.5	.015
113	14.309	.7915	11.5	.015
114	14.395	.7963	11.5	.015
115	14.481	.8011	11.5	.015
116	14.567	.8058	12.0	.015
117	14.650	.8106	12.0	.015
118	14.734	.8152	12.0	.015
119	14.817	.8198	12.0	.015
120	14.901	.8245	12.0	.015
121	14.985	.8291	12.0	.015
122	15.068	.8339	12.0	.015
123	15.152	.8385	12.0	.015
124	15.236	.8432	12.0	.015
125	15.319	.8478	12.0	.015
126	15.403	.8525	12.0	.015
127	15.485	.8571	12.0	.015
128	15.567	.8616	12.0	.015
129	15.649	.8662	12.0	.015
130	15.731	.8708	12.0	.015
131	15.812	.8753	13.0	.015
132	15.892	.8797	13.0	.015
133	15.973	.8843	13.0	.015
134	16.053	.8887	13.0	.015
135	16.133	.8932	13.0	.015
136	16.214	.8977	13.0	.015
137	16.293	.9021	12.5	.015
138	16.373	.9066	12.5	.015
139	16.452	.9110	12.5	.015
140	16.532	.9154	12.5	.015
141	16.611	.9199	12.5	.015
142	16.691	.9243	12.5	.015

a result of the desire to test large suction-velocity ratios. The pressure lines were connected to the pressure transducer by means of a Scanivalve. The water manometer data were recorded photographically. The digital voltmeter data were recorded by hand.

The porosity calibrations were made by mounting the test panels to a plenum box which was connected to the suction side of a centrifugal blower through a venturi. The venturi was calibrated prior to the porosity tests. Pressure data for the porosity tests were obtained with calibrated, sensitive airspeed instruments. It should be noted that direct measurement of the suction flow from the model was not made during the wind-tunnel test program. This direct measurement was not considered to be feasible because of the number of suction flow ducts and blowers that were used on the model. Model suction flow was determined from the measured suction plenum pressures, the model static pressures, and the porosity calibration data obtained for each size of suction hole used on the model.

DATA REDUCTION

Tunnel test dynamic pressure and velocity were determined, for each test run, from the average velocity obtained from the four sets of Pitot probes and static-pressure taps mounted on the forward section of the false walls. Tunnel flow properties were computed using the ambient temperature, measured in the test section, and the ambient pressure which was obtained from a laboratory barometer located adjacent to the tunnel. The test section was vented to the atmosphere, and the measured pressure was representative of the average static pressure at the position of the model.

The manometer board pressure data were recorded photographically. Data reduction utilized a film reader with an integral analog-to-digital converter. The digital data were processed through an IBM 360 computer to obtain the lift and moment coefficients. Moment data were referred to the leading edge of the model, and the chord of the 0°-camber configuration (16 inches) was used as the reference length for all coefficient data. Angle of attack was measured with respect to the 0°-camber chord line for all model configurations.

The hand-recorded pressure-transducer data were reduced through hand calculation. Section forces and moments were obtained by mechanical integration of the appropriate plotted data. Because some zero shift was experienced in the pressure transducer data, zero readings were taken for each test run. These zero readings were used in reducing the test data for the corresponding run. Although the zero shift in the transducer data was observed during the calibration of the transducer, no change in sensitivity was noted, and a constant sensitivity was used for all transducer data reduction.

The wake data, used to determine the model drag, were photographically recorded from a water manometer. The data were processed through the A-D converter and computations were accomplished with the digital computer. Drag coefficients were determined using Jones' method; see Reference 3.

The porosity data are given in terms of "equivalent" volume flow rate as a function of the pressure differential across the test panel. The porosity measurements were made under conditions near standard sea level, and the data are considered valid for standard conditions. Variations in porosity test conditions represented less than a 2-percent change in porosity data. The volume flow rate, at a given pressure differential across the panel, for nonstandard conditions is obtained by multiplying the "equivalent" flow rate by the square root of the density ratio (i.e., $Q = Q_{std}\sqrt{\rho_{std}/\rho}$).

The suction velocities were computed only for the chordwise locations of the static-pressure taps on the upper surface of the model. The model suction-hole size and spacing at, or adjacent to, the position of the static-pressure tap and the corresponding computed pressure differential, across the model skin, were used to determine the suction flow rate for a 1-foot length of suction holes. Suction velocity was obtained by dividing the computed volume flow rate by the effective area of the row of suction holes. This effective area was defined as the product of the surface distance between lines halfway between adjacent rows of suction holes and the reference span, which was 1 foot. The suction velocity ratio used the local velocity obtained from the static-pressure data and the test suction velocity.

DISCUSSION AND RESULTS

THEORETICAL ANALYSIS

The following paragraphs describe the method used to compute the suction-velocity distribution intended to prevent flow separation on the wind-tunnel suction model. The design maximum section lift coefficient was chosen to be 4.9 with 30° camber. This value was somewhat arbitrary, but was considered to be possible in light of the successful utilization of distributed-suction boundary-layer control on earlier test aircraft. Section lift coefficients of the order of 4.0 were obtained on the high-lift L-19 aircraft (see Reference 1) which did not have the advantage of the variable-camber wing configuration. A free-stream velocity of 80.0 feet per second was assumed for the suction-velocity calculations.

The pressure distribution for the suction calculations was obtained with the perfect-fluid method of Theodorsen as modified for viscous effects by Pinkerton; see Reference 4. Reasonable agreement between this method and experimental pressure distributions was obtained from data taken on the high-lift L-19 aircraft. Comparisons with test data obtained in the present program are shown in Figures 29 and 30 and are discussed in a later paragraph. The resulting velocity-ratio distribution for the upper surface of the model at the design lift coefficent is shown in Figure 4.

The computation of the development of the boundary layer along the impervious surface of the model was accomplished with the method of Truckenbrodt, Reference 5. Another method, described below and also using the momentum and energy integral equations, was used for the sucked areas of the model surface. The criterion used to forestall separation of the turbulent boundary layer was that the boundary-layer shape parameter, H_{12}, not be allowed to exceed a value of 1.7. This value is conservative considering the normally used separation criteria of from 1.8 to 2.2. The transition of the laminar boundary layer was assumed to take place at the peak value of the potential-flow velocity ratio. This transition point was at the leading edge of the airfoil for the design lift coefficient. The impervious surface calculations were performed on a digital computer (the program, which follows the method of Reference 5, is described in Reference 6). The suction velocities were determined by hand calculations.

The computation procedure was to initially compute the development of the boundary layer, without suction, starting at the forward, potential-flow stagnation point. These results defined the location along the upper surface of the airfoil at which the values of H_{12} first exceeded 1.7 and provided the initial conditions for the suction calculations. The calculation of the suction velocities and the sucked boundary-layer characteristics was

then started and continued until the computed suction velocities became negative. The impervious calculations were again started, with the appropriate initial conditions from the suction calculations, and continued until the value of H_{12} again exceeded 1.7. The suction calculations then were performed until the trailing edge of the airfoil was reached.

The method used to compute the suction velocities was based on the momentum integral equation

$$\tau_w/\rho U^2 = (H_{12} + 2) \quad (\delta_2/U)\, dU/dS + d\delta_2/dS + v_s/U \tag{1}$$

and the energy integral equation

$$2(d_1 + t_1)/U^3 = [d(U^3\delta_3)/dS]/U^3 + v_s/U \tag{2}$$

The assumptions and empirical relationships used in solving this set of equations were similar to those used by Truckenbrodt except for the changes required to compensate for the additional unknown, v_s, and its effect on the other terms of the equations. Specifically, it is known that the presence of suction has an influence on the wall shearing stress, τ_w, and the energy dissipation, d_1. Since the relationship between H_{12} and H_{32}, used by Truckenbrodt and based on the results of J. Rotta, was based on boundary-layer data without suction, it was anticipated that suction might also change this relationship. The only suitable data found to provide information on the influence of suction on these variables, particularly for rows of discrete suction holes, were due to Wuest (Reference 7). Wuest showed that the impervious relationship between H_{12} and H_{32} is also valid for the sucked boundary layer. He also showed, with limited data and for the values of H_{12} tested, that the increase in energy dissipation due to the presence of suction is of the same order of magnitude as the increase in wall shearing stress. One other reference pertaining to the effect of suction on the wall shearing stress was Reference 8, where an expression

$$\tau_w/\rho U^2 = A(1 + 100\, v_s/U)/R_{\delta 2}^{0.268} \tag{3}$$

where

$$A = 0.123 \times 10^{-0.678 H_{12}}$$

is given. This expression was apparently suggested by Sarnecki and is an extension of the expression suggested by Ludwieg and Tillman in Reference 9 and used by Truckenbrodt. Equation (3) was used for the present suction velocity calculations even though the increase in shear stress due to suction is less than that shown by Wuest. In light of the limited success obtained with this method of computing the suction velocities, this was possibly a questionable choice; but at the time of the computations, the limited data available did not seem to justify significant changes to Equation (3). Wuest also indicated a dependence of the increase in shear stress due to suction on the values of H_{12}, but the limited data shown also made an attempt to include this effect questionable.

For the impervious case, Truckenbrodt has suggested the expression

$$(d_1 + t_1)/\rho U^3 \cong d_1/\rho U^3 = 0.0056/R_{\delta 2}^{1/6} \qquad (4)$$

for the energy dissipation, where the dependence upon H_{12} and the magnitude of the turbulent energy, t_1, are neglected. To be consistent with the data of Wuest, Equation (4) should have been modified by a factor as used in Equation (3) to account for the effects of suction. It turns out, however, that a change to the factor used in Equation (3) allows the elimination of the suction velocity between Equations (1) and (2) so that the momentum thickness, δ_2, may be solved for directly. This simplification was utilized in these suction-velocity calculations, where it was assumed that

$$2(d + t)/\rho U^3 = B(1 + 100A\ v_s/BU)/R_{\delta 2}^{0.268} \qquad (5)$$

The value of B was chosen to provide a match with Equation (4) for the impervious case and at the Reynolds number of interest (i.e., to compensate for the change of the exponent of $R_{\delta 2}$). Values of 0.02 ($R_{\delta 2}$ of the order of 10^2) and 0.0256 ($R_{\delta 2}$ of the order of 10^4) were used for B at the leading edge and more aft locations respectively in the suction-velocity calculations.

The use of Equations (3) and (5) still leaves an excess of unknows for the system of equations; this deficiency was avoided by assuming that H_{12}, and therefore H_{32}, remains constant over the sucked portion of the airfoil. Some support for this assumption is found in Reference 1, where relatively small changes in H_{12} were measured along the surface of the sucked airfoil. A constant value of 1.7 was used for H_{12} in the present suction-velocity calculations. With the number of unknowns reduced to two, δ_2 and v_s, v_s was first eliminated between Equations (1) and (2) to give

$$d\delta_2/dS + (C\delta_2/1.268U)\ dU/dS = (B - A)R_{\delta 2}^{-0.268/(H_{32}-1)} \qquad (6)$$

where

$$C = 1.268\ (3H_{32}-H_{12}-2)/(H_{32}-1)$$

This equation can be solved directly, giving

$$\delta_2^{1.268} = [\delta_{2_o}^{1.268}(U_o/U_\infty)^C + DcU_\infty^{-0.268}\int_{S/S_t|_o}^{S/S_t} (U/U_\infty)^{C-0.268} d(S/S_t)]/(U/U_\infty)^C \qquad (7)$$

where

$$D = 1.268\ (B-A)\nu^{0.268}/(H_{32}-1)$$

Eliminating $d\delta_2/dS$ from Equations (1) and (2) provides the solution for the required suction velocity as a function of the value of δ_2 determined from Equation (7).

$$v_s/U =$$

$$(AH_{32}-B-H_{32}(H_{12}-1)R_{\delta 2}{}^{0.268}(\delta_2/U)dU/dS)/(H_{32}-1)(R_{\delta 2}{}^{0.268}-100A) \qquad (8)$$

The suction velocities computed for the model at a lift coefficient of 4.9 and a tunnel velocity of 80 feet per second are shown as a function of the surface-distance ratio in Figure 5. The suction velocities computed using the method of R. Eppler (Reference 10) are also shown in this figure. The Eppler values were used to gain insight into the range of values of suction velocity that different prediction methods give and were the basis for reducing the level of suction, over that computed by the above method, initially applied over the rear portion of the model at the design level of internal suction pressure. The idea was to use a lower value of suction velocity on the aft portion of the airfoil to allow for possibly over-conservative values being provided by the design method. At the same time, the maximum level of suction available on the model allowed the higher, computed values to be realized at the expense of oversucking the forward portion of the aft suction area. The curves shown in Figure 5 give the anticipated range of suction velocities for the final suction-hole distribution that would have been available if the design lift coefficient had been realized in the tunnel.

The maximum lift coefficient obtained in the suction-model wind-tunnel test was 3.6. This value was considerably short of the design value of 4.9 and implies that the above method of computing the required suction velocities is inadequate or that one, or more, of the assumptions used is inappropriate. Unfortunately, due to problems encountered during the test program, there was insufficient time available to recompute, with this method, the suction velocities required to obtain a lift coefficient of 3.6. Such calculations would have provided needed insight into the specific deficiencies of this method. One likely source of error, however, is the magnitude of the increase in wall shear stress due to suction. More recent test data obtained on the wing of the high-lift L-19 aircraft (Reference 11) indicate that the factor of 100 used in Equation (3) should be as high as 500. This value is in rough agreement with the data given by Wuest and has a significant effect on the resulting computed values of suction velocity. With a corresponding change in Equation (5), a change from 100 to 500, assuming $R_{\delta 2} = 4000$ and $H_{12} = 1.7$, would increase the computed suction velocity by 70 percent. It should be noted that the higher value of the suction factor (500) was obtained from measured boundary-layer data, and it was assumed that the momentum integral equation adequately represents the relationships between the various boundary-layer parameters. The same assumption is inherent in the data of Wuest. This is an area in which more extensive and closely controlled test data are needed.

IMPERVIOUS MODEL TEST DATA

The test results for the impervious model are presented and discussed in the following paragraphs. All data, including the suction model data given later, are referred to the 0°-camber chord line with the pitching-moment data measured with respect to the leading edge of the 0°-camber chord line. Boundary-layer transition strips were not used with this impervious model.

The chordwise pressure distributions, in terms of pressure coefficient, as a function of the fractional distance along the 0°-camber chord line are shown in Figures 6 through 17 for the 0°-, 5°-, and 10°-camber configurations. Data for 0°, 8°, 16°, and 20° angle of attack are shown for the 0°- and 5°-camber configurations and 0°, 8°, 16°, and 18° angle of attack are shown for the 10°-camber configurations.

The variation in measured lift coefficient as a function of angle of attack for the 0°-, 5°-, and 10°-camber configurations is shown in Figures 18 through 20. Values of lift coefficient obtained from the two model-span stations are shown to indicate the degree of two-dimensionality that was achieved with this model. The lift characteristics, as well as tuft observations, show a gentle progressive trailing-edge stall pattern with the camber angles used in the impervious test.

The pitching moment characteristics for the 0°-, 5°-, and 10°-camber configurations are shown as a function of lift coefficient in Figures 21 through 23. The model aerodynamic center, as determined from the slope of the pitching-moment-coefficient to lift-coefficient line, is at 27 percent of the 0°-camber chord for these configurations. A very mild amount of pitchup, consistent with the trailing-edge stall pattern, is noted at stall.

The drag data, obtained through wake momentum-loss measurements, were very erratic. These data were also inconsistent with the level of drag measured on a glove section model of the 0°-camber configuration (Reference 12) and the published data for the 63_2-615 airfoil from which the variable-camber airfoil configuration was derived (Reference 13). The scatter in the data obtained from a single camber configuration obscured any observed variations between data for different configurations and made any comparative drag analysis meaningless. For this reason, no drag data are shown in this report.

In general, the impervious test data show that the changes in section characteristics are similar to those that would be expected with small deflections of a plain trailing-edge flap. It was anticipated that some improvements in lift-to-drag ratio at higher values of lift coefficient might be realized with the variable-camber configurations, but the lack of valid drag data prevents any such conclusion.

POROSITY DATA

The suction-hole porosity characteristics were measured by using a series of test panels. Sheets of 0.020-inch aluminum, as used for the

model skins, were used as the test panels. One hundred and twenty suction holes, of a given size, were drilled in each panel. Suction holes of 0.007-, 0.010-, 0.015-, and 0.018-inch diameter were tested. The test panels were mounted in the test fixture so that the suction flow passed through the holes in the same direction as the holes were drilled. This was the same relationship that existed with the model where the suction holes were drilled after the model was assembled. The outer surface of the test panels and the model was finished with fine abrasive cloth after the holes were drilled.

No testing was conducted to determine the effect of an external crossflow on the panel porosity characteristics. Wuest (Reference 7) presented data to indicate that an external flow of 130 feet per second reduced the value of measured porosity by 20 percent as compared to the porosity measured with no external flow. Wuest's data were for 0.079-inch-diameter suction holes drilled in metal of undefined thickness. Ward (Reference 14) obtained a 4-percent reduction for 0.040-inch-diameter suction holes in 0.040- or 0.025-inch-thick aluminum with an external crossflow of 60 feet per second. Earlier, unpublished porosity measurements made at Mississippi State University gave results which placed the effect of crossflow within the accuracy band of the porosity measurement for hole diameters less than 0.025 inch. Although there seems to be ample evidence that external crossflow results in some reduction in measured porosity, these data seem to indicate that this effect should be small for the suction holes used in the present program. No external crossflow correction was applied to the test data shown in this report.

The resulting porosity curves used in the analysis of the tested suction model are shown in Figure 24. These results are for 120 suction holes and represent volume flow rates for standard atmospheric conditions.

SUCTION MODEL TEST DATA

Two series of suction tests were conducted on the 30°-camber configuration (suction model). The initial test used the suction model with the 4 rows of leading-edge suction holes and 108 rows of aft suction holes. The aft suction holes extended from a surface distance of 6.324 inches aft of the leading edge (x/c = 0.3449) to 16.691 inches aft of the leading edge (x/c = 0.9243). Pressure data were measured by means of water manometers for the first series of tests. In addition to the fact that the design lift coefficient was not realized in these tests, the test data accuracy was considered to be marginal at the lower test speeds that were used to obtain large suction-velocity ratios on the model. In this first series of tests, the start of separation occurred at around 9° angle of attack. A boundary-layer transition strip, consisting of a narrow strip of abrasive powder bonded to the surface forward of the first row of leading-edge suction holes, was used on both series of suction tests to insure that some form of leading-edge separation bubble was not present on the model.

A pressure transducer, Scanivalve and digital voltmeter were added to the test equipment for the second series of suction tests. In addition to the

improved pressure instrumentation, the aft suction distribution was extended for the second test. The first row of aft suction holes was now located 3.495 inches (surface distance) aft of the leading edge of the model. This distance corresponded to a chord ratio of 0.1861. A total of 138 rows of suction holes were provided in this final, aft suction distribution. All of the suction model test data shown in this report are for this final suction-hole distribution and the improved pressure measuring system. No attempt was made to obtain drag data during the suction test because of the poor results experienced during the impervious model test.

The objective of the suction test was to obtain test data for two suction conditions at each angle of attack and tunnel speed tested. The first suction test condition was the maximum suction available on the model, and the second condition was the lowest level of suction for which the same model pressure distribution, as was obtained with maximum suction, could be maintained. Since the direct model loads were not available in this test program, it was necessary to use the surface pressure from a limited number of pressure taps as an indication of the integrated lift force on the model. It was found that the static-pressure tap located at $x/c = 0.04$ gave the most noticeable indication of an impending loss of lift as a result of separation on the aft portion of the model. The test technique first involved obtaining the desired maximum-suction data. The leading-edge suction was then reduced to a level slightly above the value that changed the reference tap ($x/c = 0.04$) reading. With this leading-edge suction setting, the aft suction was reduced to a level that was slightly above a setting that produced a change in the reference tap reading. The two suction settings were then readjusted to see if additional reductions could be used without changing the reference tap reading. As the optimum-suction static-pressure data were being recorded, the values were checked against the corresponding maximum-suction data to insure that the two pressure distributions were indeed the same.

The pressure distribution data for the 30°-camber suction model are given for angles of attack of 8°, 12° and 15° in Figures 25 through 27. These data are for the maximum available suction, although they are equally representative of the optimum-suction data. These data are for the low tunnel speed, nominally 54 feet per second, which gave a test Reynolds number, based on the 16-inch chord, of 0.47×10^6. The potential-flow results for the angles of attack nearest the test conditions are also shown in Figures 25 and 26. No comparison between theory and experiment is shown for 15° angle of attack, since separation was observed at this test condition. The most significant differences between the theoretical and the experimental results are the lower leading-edge pressures (less negative pressure coefficients) shown by the model and the smoother upper-surface adverse pressure gradient given by the theoretical results. The lower leading-edge pressures may be due to boundary-layer effects on the model or problems with the conformal representation of the leading edge of the model in the theoretical method. No reason is offered for the midchord differences in the pressure data. In terms of the effect of the use of the theoretical pressure distribution in computing the required suction

velocities, the higher leading-edge static pressure and the resulting increase in pressure gradients should give conservative results. The difference in the midchord pressure distribution could possibly result in underestimating the required suction when using the theoretical method.

The lift coefficient characteristics of the suction model are shown as a function of angle of attack in Figures 28 and 29. Figure 28 presents the data for the lower test speed and, in addition to showing the data for the maximum and optimum suction, gives the results for maximum aft suction with the leading-edge suction holes sealed. The benefits of the leading-edge suction are observed only at angles of attack exceeding 9°. The differences in lift coefficient shown for maximum and optimum suction at a given angle of attack are considered to be within the scatter of the test data. The higher speed data shown in Figure 29 indicate the reduction in the effectiveness of the boundary-layer control system due to the resulting lower values of suction-velocity ratio. Although the design lift coefficient was not achieved with the tested configuration, the maximum lift coefficient of 3.6, obtained at a Reynolds number of 0.47×10^6, is an impressive measure of the potential capabilities of a distributed-suction boundary-layer control system. The developed maximum lift coefficient was limited by the particular suction system used in this test. Improvements in the level and/or distribution of suction would undoubtedly result in higher test values of the maximum lift coefficient.

The pitching moment data for the suction model are presented in Figures 30 and 31 for the low and high test speeds respectively. Only data for maximum suction are shown. The moment characteristics are similar to those found with most high-lift trailing-edge devices. A small amount of pitchup is seen at stall.

The relationship between the maximum suction available and the optimum suction setting and some insight into the significance of the levels of suction used in this test are provided by considering the internal wing pressures (suction plenum pressures) corresponding to those suction settings. Figures 32 and 33 show the variation of the leading-edge and aft suction plenum pressures as a function of model angle of attack. The data in Figure 32 are for the low-speed test, and the higher test-speed data are shown in Figure 33. The solid and dashed curves represent the static-pressure readings of the upper surface pressure taps located at chord ratios of 0.01 and 0.30 respectively. These pressure taps were located near the start of the leading-edge and initial aft suction distribution, and an internal pressure below (less negative) the corresponding static-pressure tap value is an indication of outflow from the initial rows of suction holes. Although this presentation neglects the changing suction distribution as internal pressure or angle of attack is changed, it is felt that it provides an indication of the physical limitations of the boundary-layer control system as tested.

In Figure 32, the upper plot indicates that the leading-edge suction did not contribute to the suppression of flow separation below angles of attack of 9°. The optimum suction setting, below 9° angle of attack, was that which prevented outflow from the suction holes. This fact was also noted from the lift data discussed previously. Since amounts of leading-edge suction greater than the optimum value did not prove advantageous, the limitation on the maximum developed lift coefficient did not seem to be the result of inadequate leading-edge suction. It was also noted during this test that a higher than optimum setting on the leading-edge suction did not result in any measurable change in the optimum aft suction setting. The lower plot in Figure 32 indicates that the maximum aft suction flow, or possibly the suction distribution at the maximum setting, was unable to retard the growth of the turbulent boundary layer and its eventual separation at angles of attack greater than 14 degrees. Similar conclusions are derived from the nigher speed data shown in Figure 33. Figure 33 indicates that the significance of the leading-edge suction was somewhat less than in Figure 32 and that the optimum aft suction settings were nearer to the maximum available setting for most of the range of angles of attack tested. It should be noted that the optimum suction settings were less reliable near, and beyond, the stalling angles of attack due to the fluctuations that appear in the static-pressure readings in this region of operation.

The computed experimental suction velocities, based on the optimum suction settings at the indicated angles of attack, are shown in Figures 34 and 35 for the low and high speeds respectively. The data are shown for angles of attack at which the flow was attached and are presented in terms of 0°-camber chord ratio. The somewhat inconsistent change in suction velocity with angle of attack, shown in Figure 34, is a result of the scatter in the optimum internal-wing pressure data with angle of attack seen in Figure 32.

CONCLUSIONS

1. Although the design lift coefficient of 4.9 was not realized on the model tested, the value of 3.6, obtained at a relatively low Reynolds number of 0.47×10^6, is considered to be significant. It is felt that significantly higher values can be shown with a suction distribution based on more valid relationships between boundary-layer variables.

2. A probable cause of the inadequate suction distribution was the use of an expression for the increase in wall shear stress, due to suction, which underestimated the effect of suction.

3. More extensive and closely controlled testing is required to properly define the effect of suction on the boundary-layer variables.

4. Possible lift-to-drag ratio improvements through the use of a variable-camber wing may be available, but no supporting data were provided by this test program.

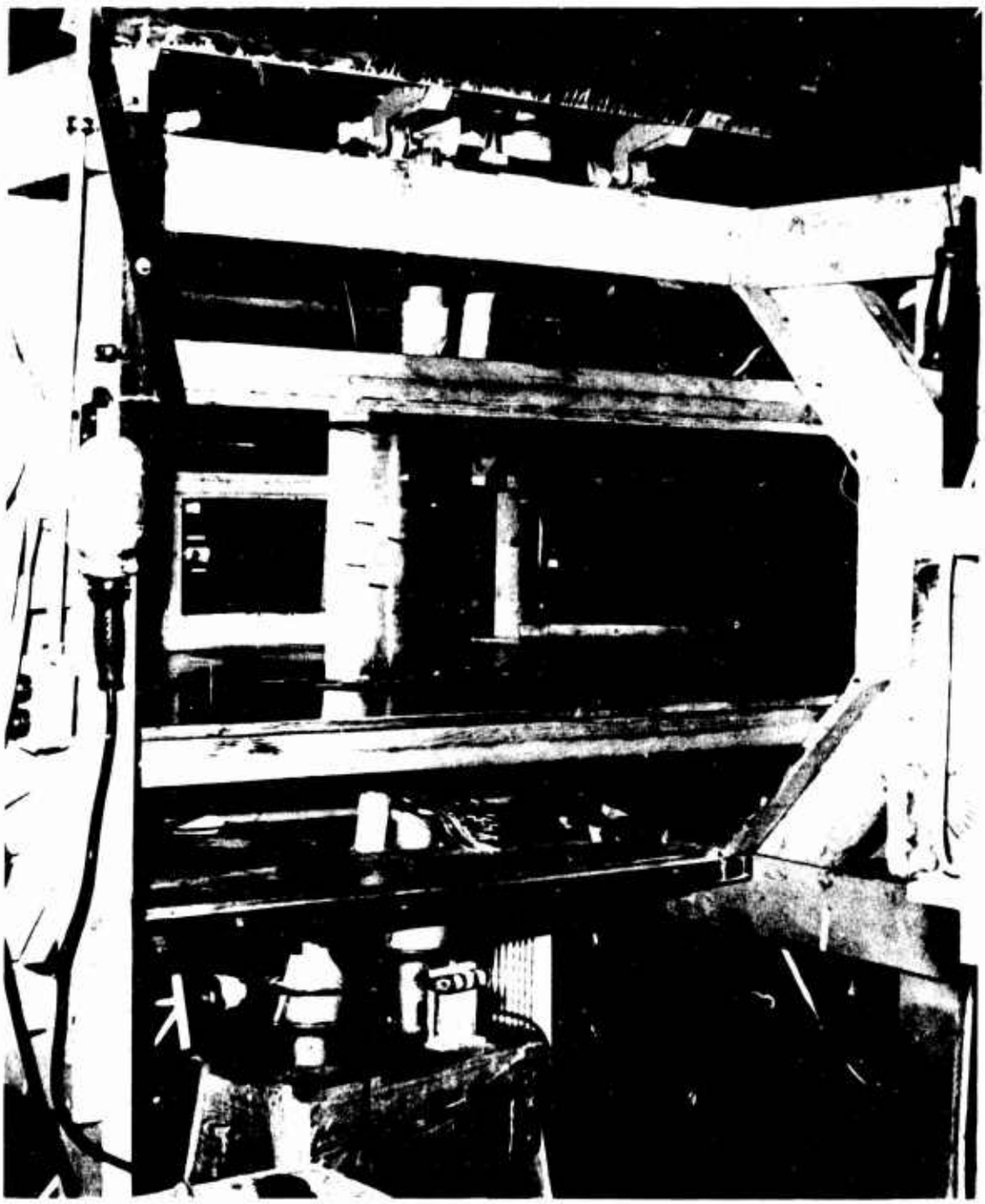

Figure 1. Wind Tunnel Installation of Suction Model.

Figure 2. Variable-Camber Model in 0^{o}-Camber Configuration.

Figure 3. 30^{o}-Camber Suction Model.

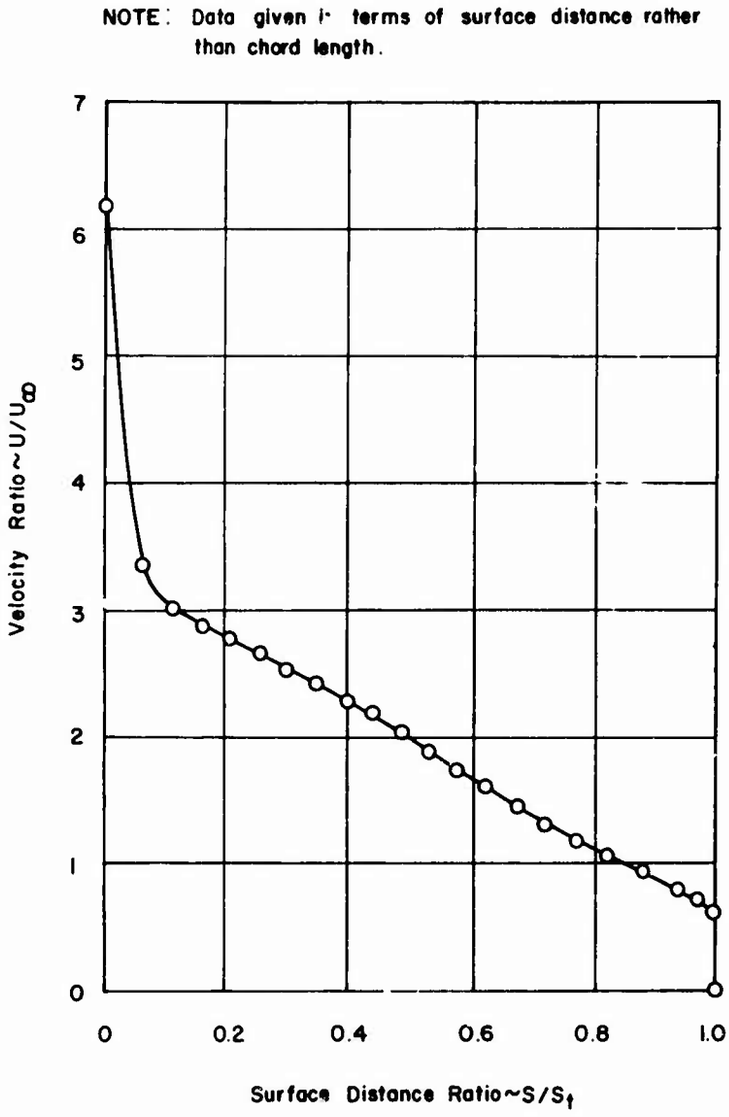

Figure 4. Theoretical (Potential Flow) Velocity Ratio Distribution for Upper Surface, C_1 = 4.9, α = 21.5°, 30° Camber.

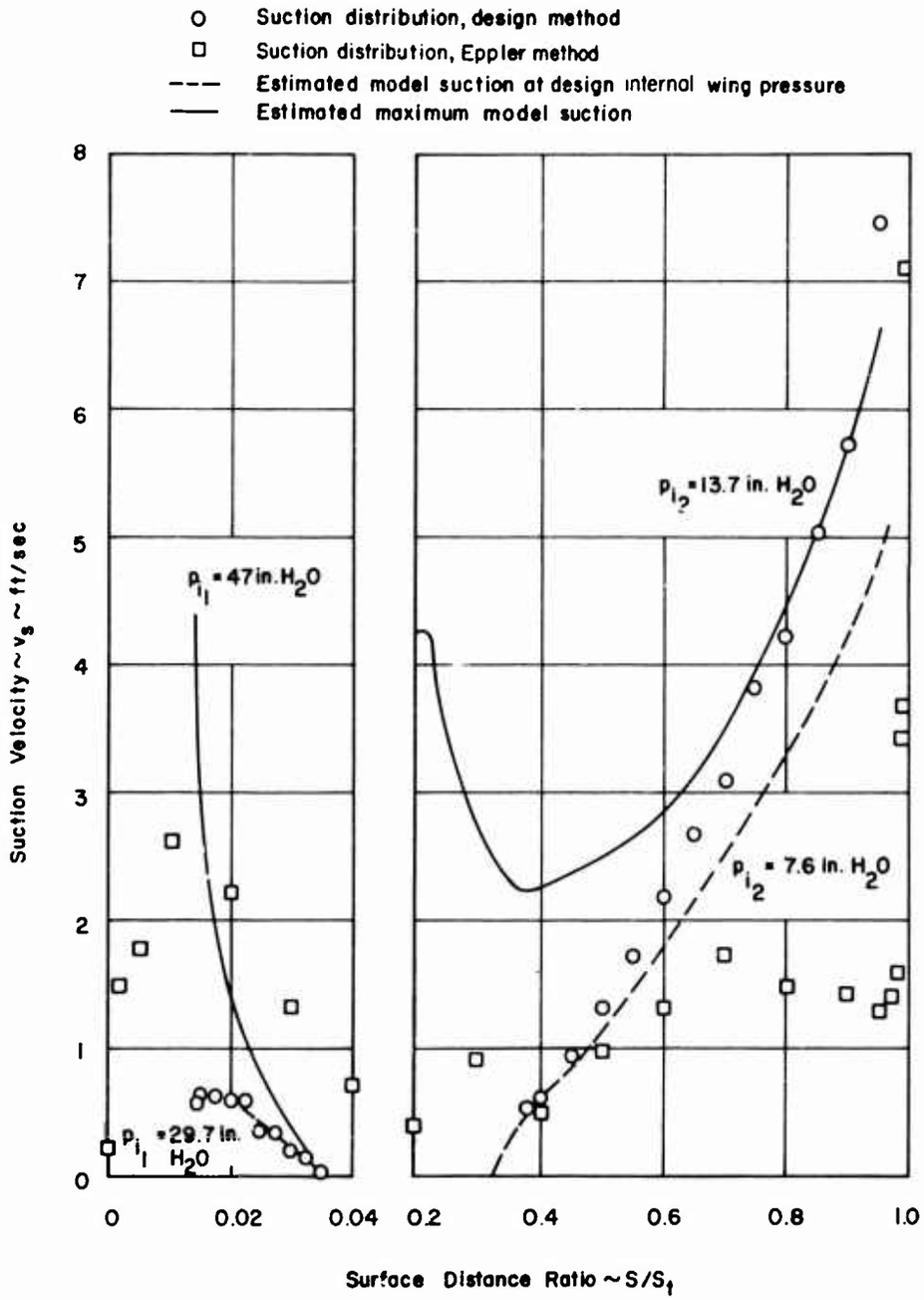

Figure 5. Theoretical Suction Distribution, C_l = 4.9, α = 21.5, 30^0 Camber.

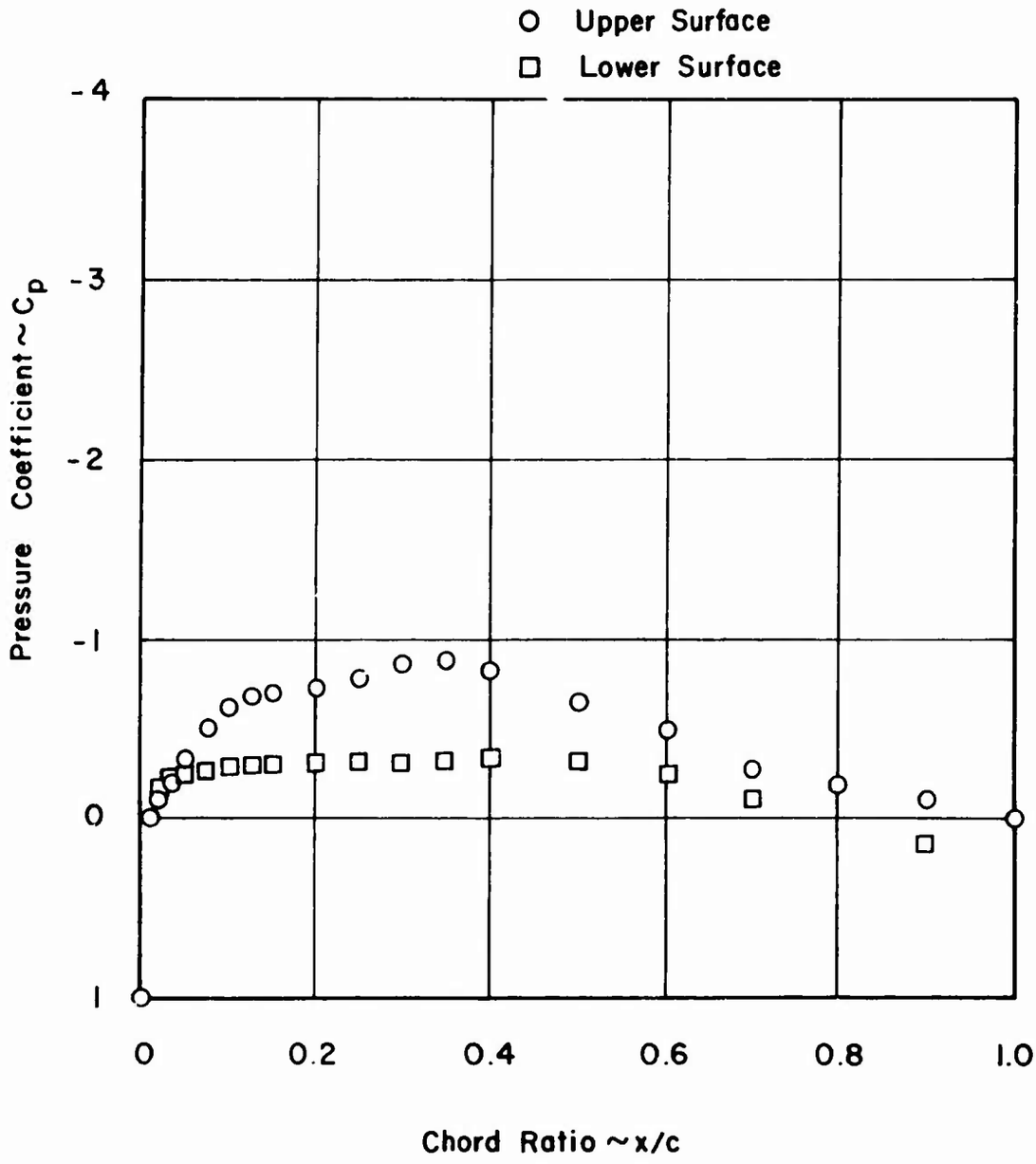

Figure 6. Pressure Distribution, Impervious Model, 0^o Camber, $\alpha = 0^o$.

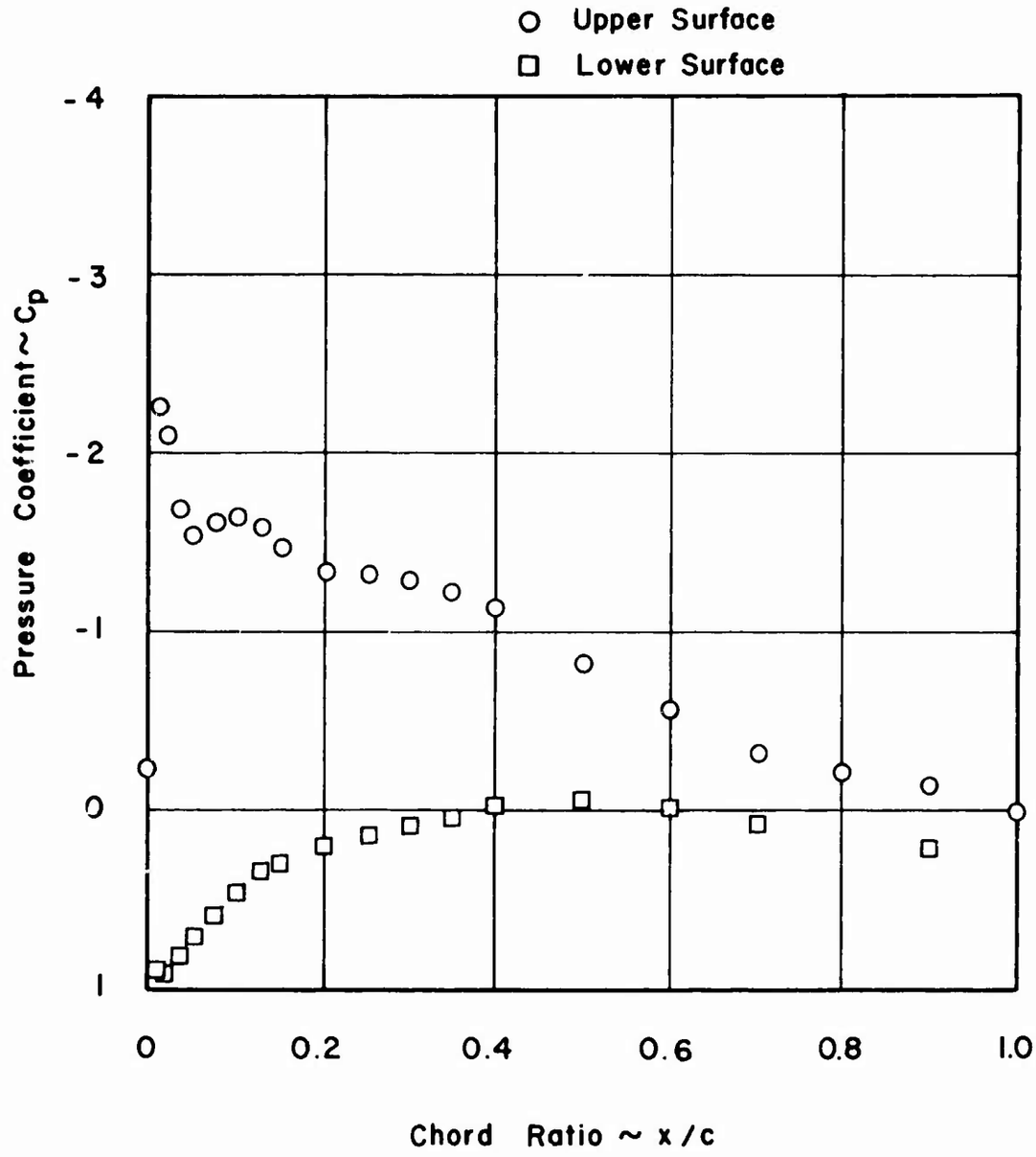

Figure 7. Pressure Distribution, Impervious Model, 0^0 Camber, $\alpha = 8^0$.

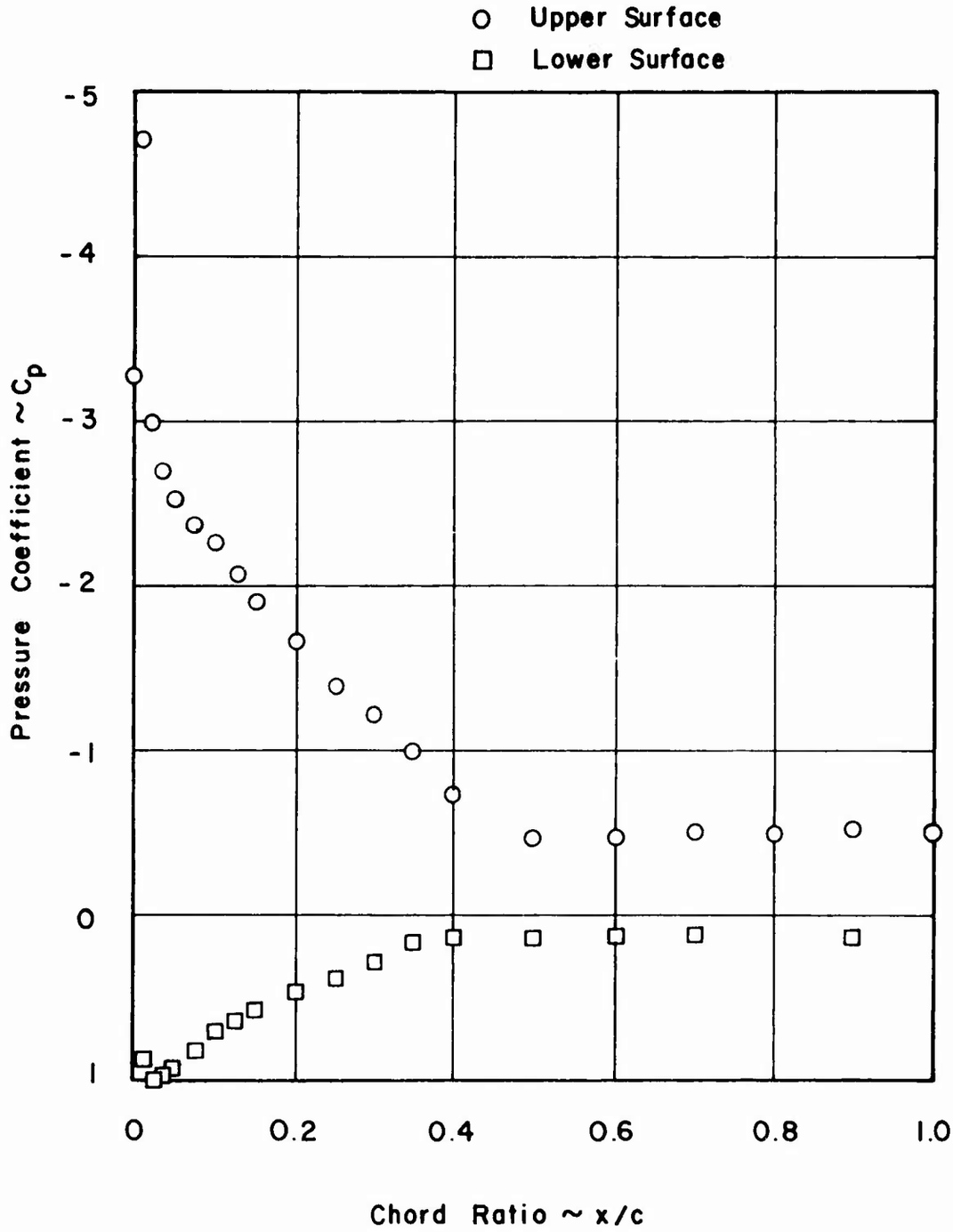

Figure 8. Pressure Distribution, Impervious Model, 0^0 Camber, $\alpha = 16^0$.

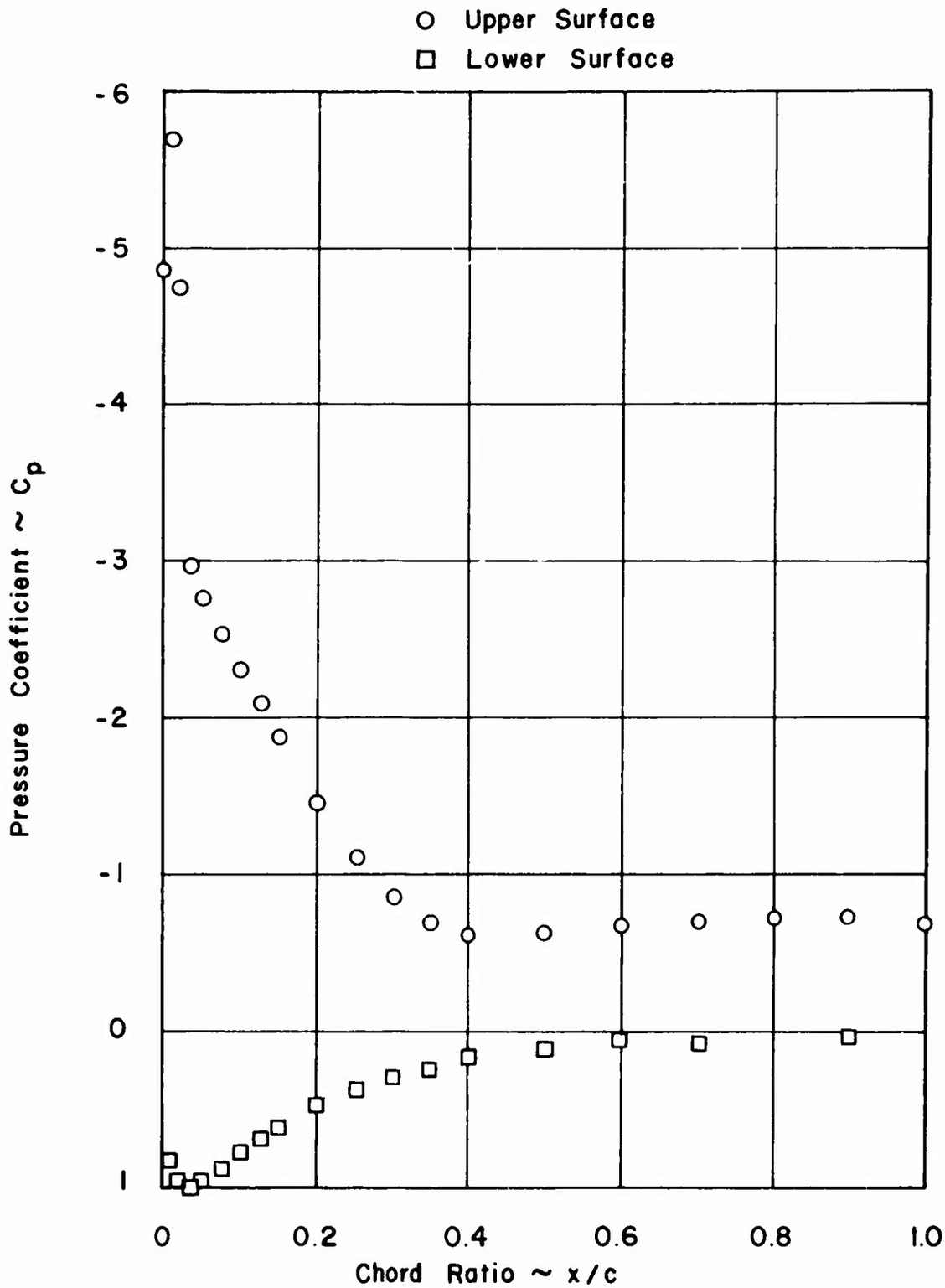

Figure 9. Pressure Distribution, Impervious Model, 0^{o} Camber, $\alpha = 20^{o}$.

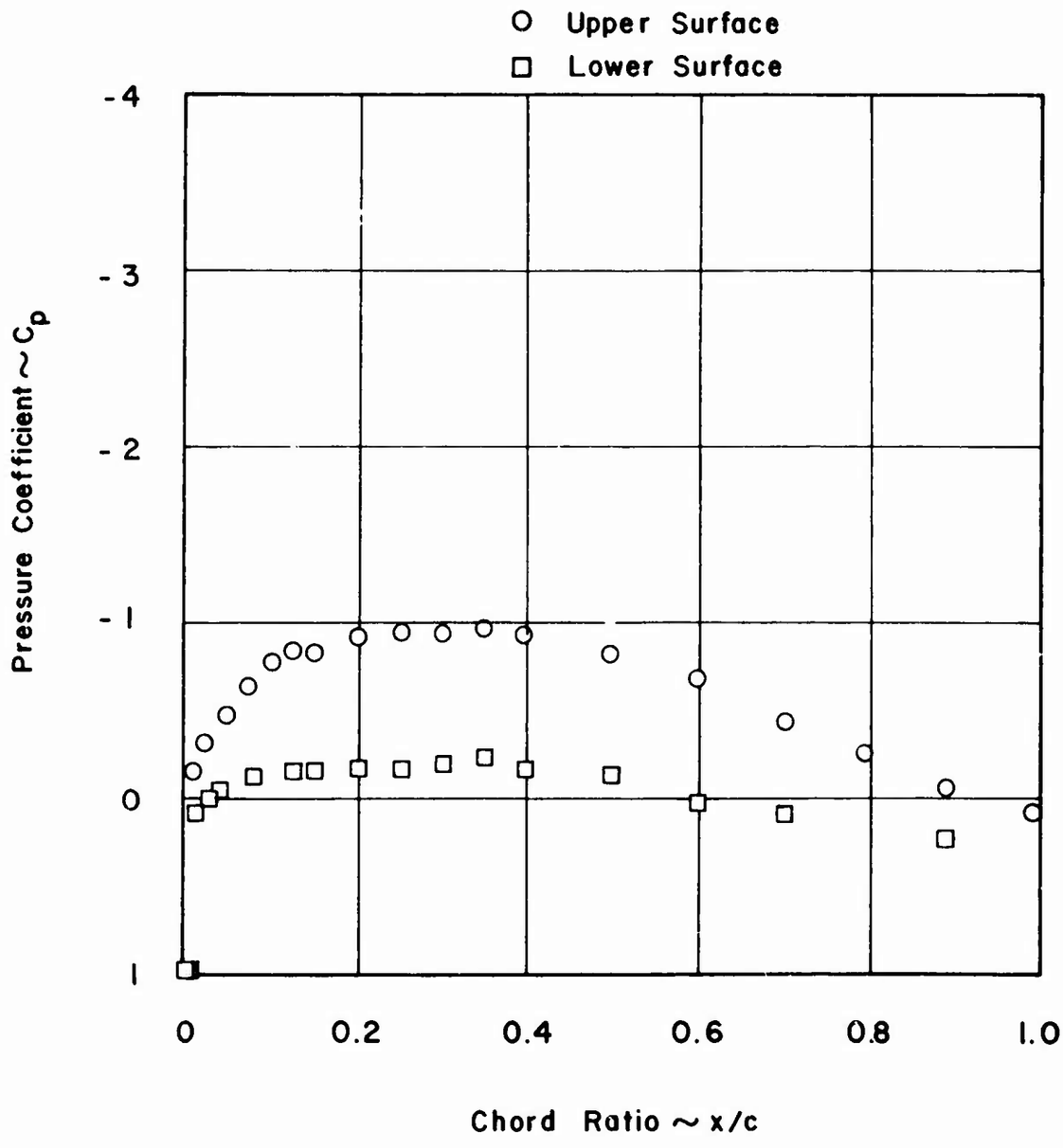

Figure 10. Pressure Distribution, Impervious Model, 5^0 Camber, $\alpha = 0^0$.

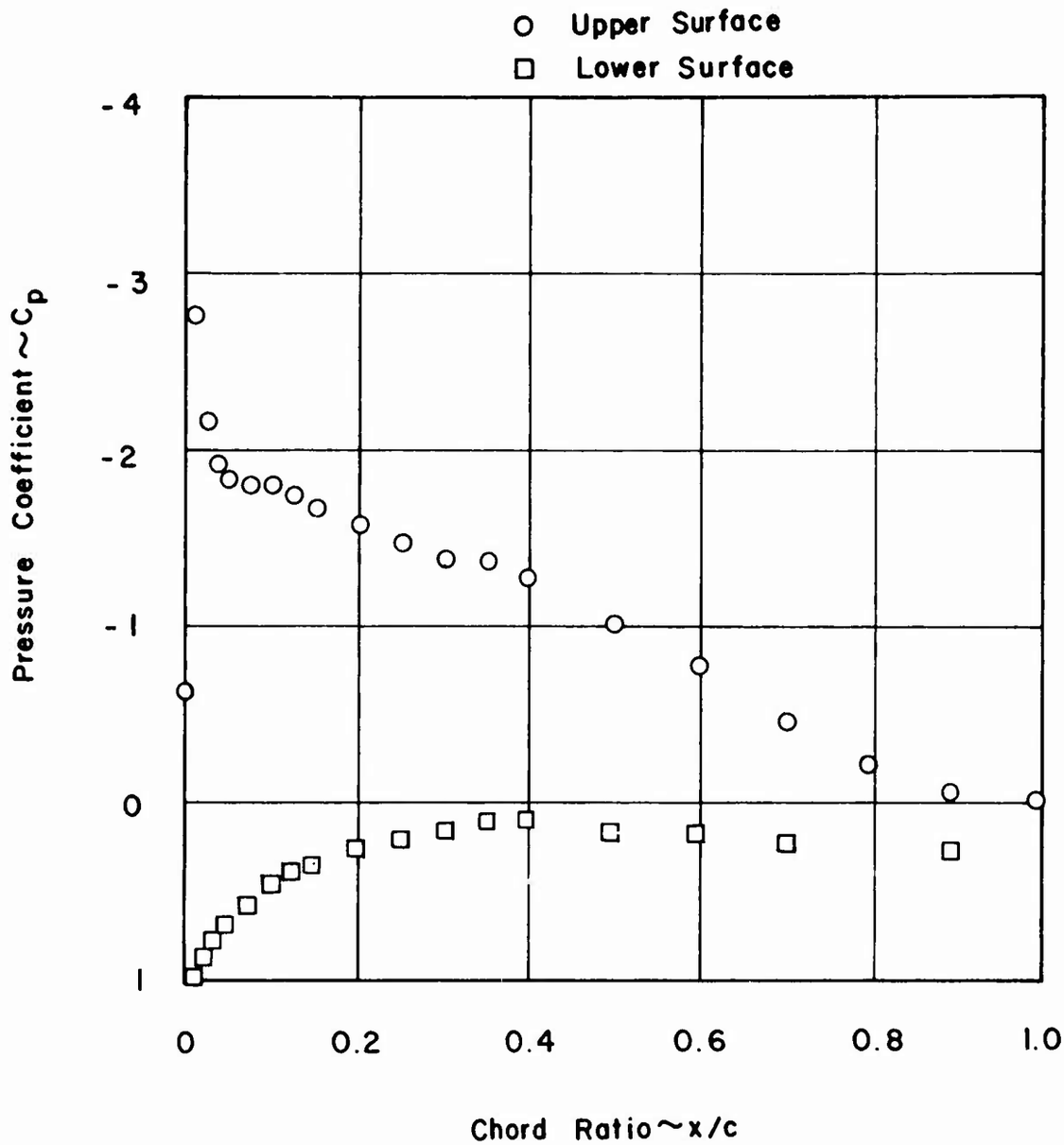

Figure 11. Pressure Distribution, Impervious Model, 5^{o} Camber, $\alpha = 8^{o}$.

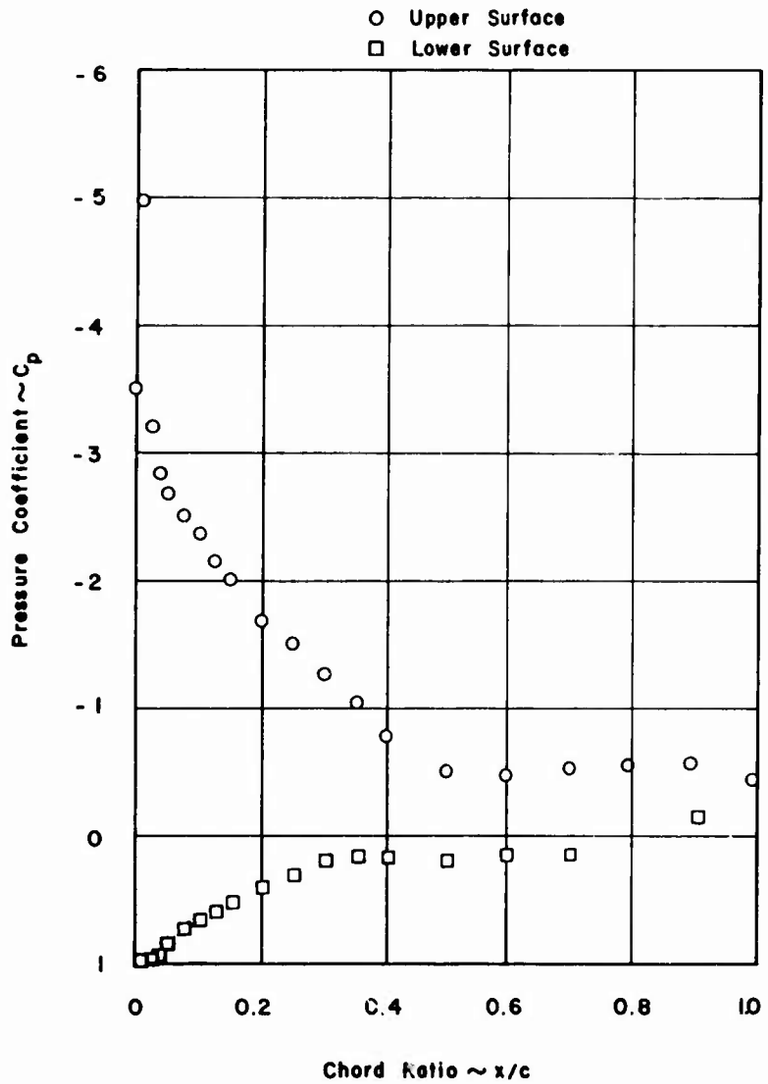

Figure 12. Pressure Distribution, Impervious Model, 5^0 Camber, $\alpha = 16^0$.

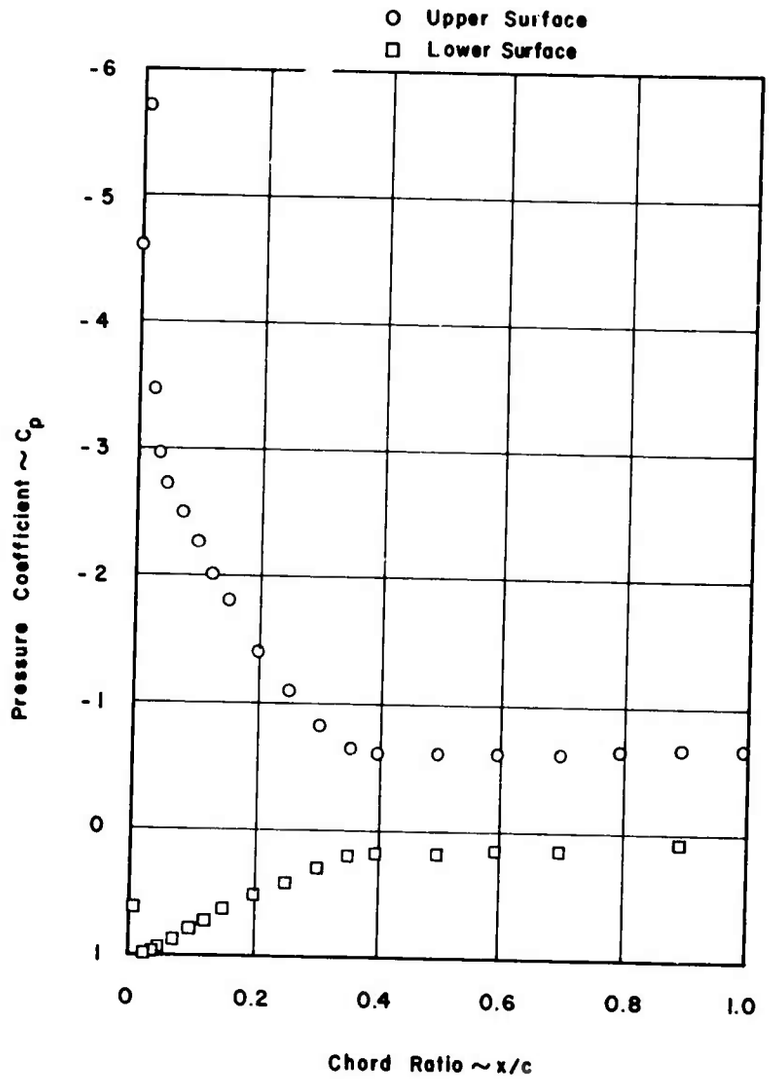

Figure 13. Pressure Distribution, Impervious Model, 5^{o} Camber, $\alpha = 20^{o}$.

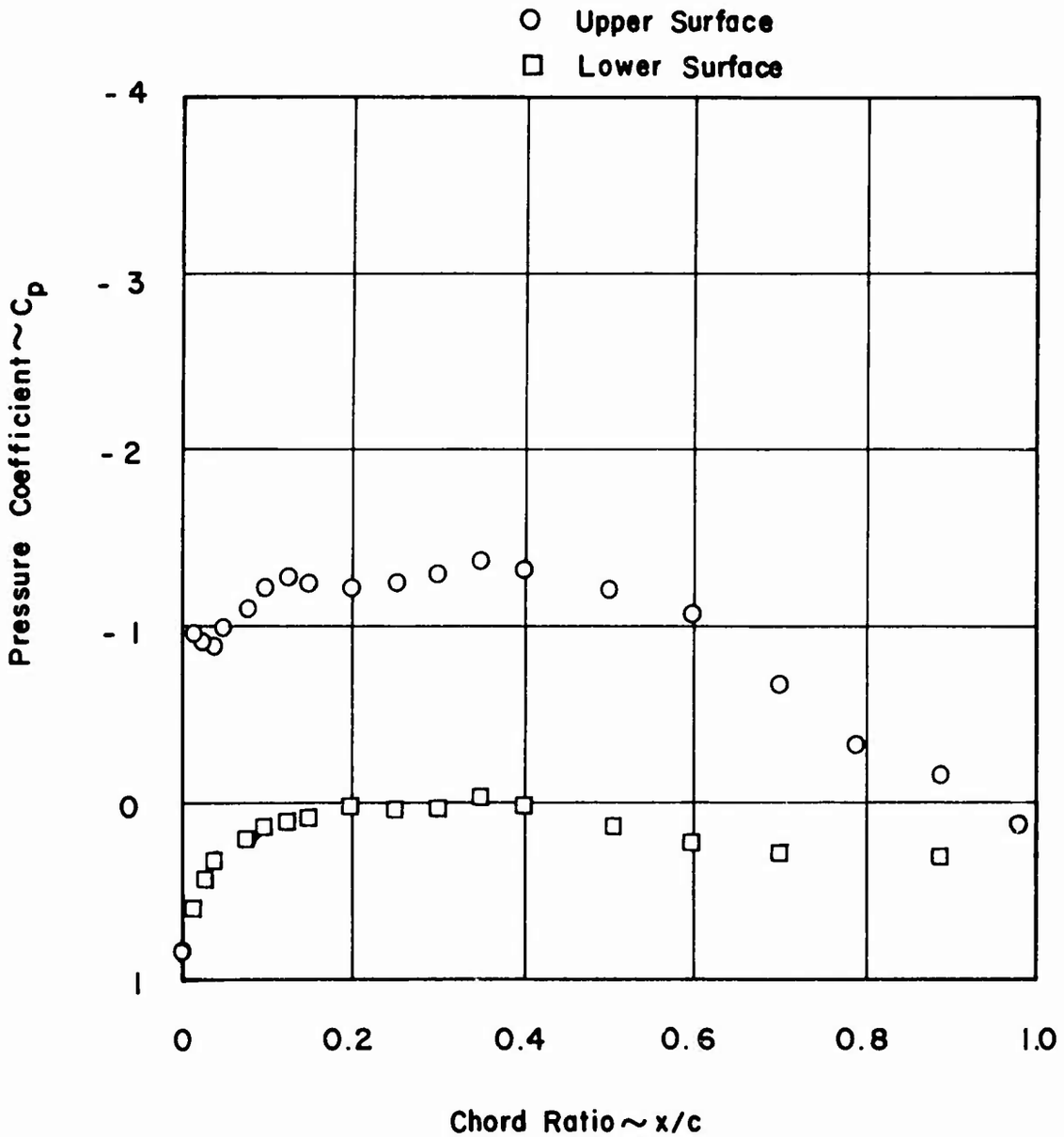

Figure 14. Pressure Distribution, Impervious Model, 10^0 Camber, $\alpha = 0^0$.

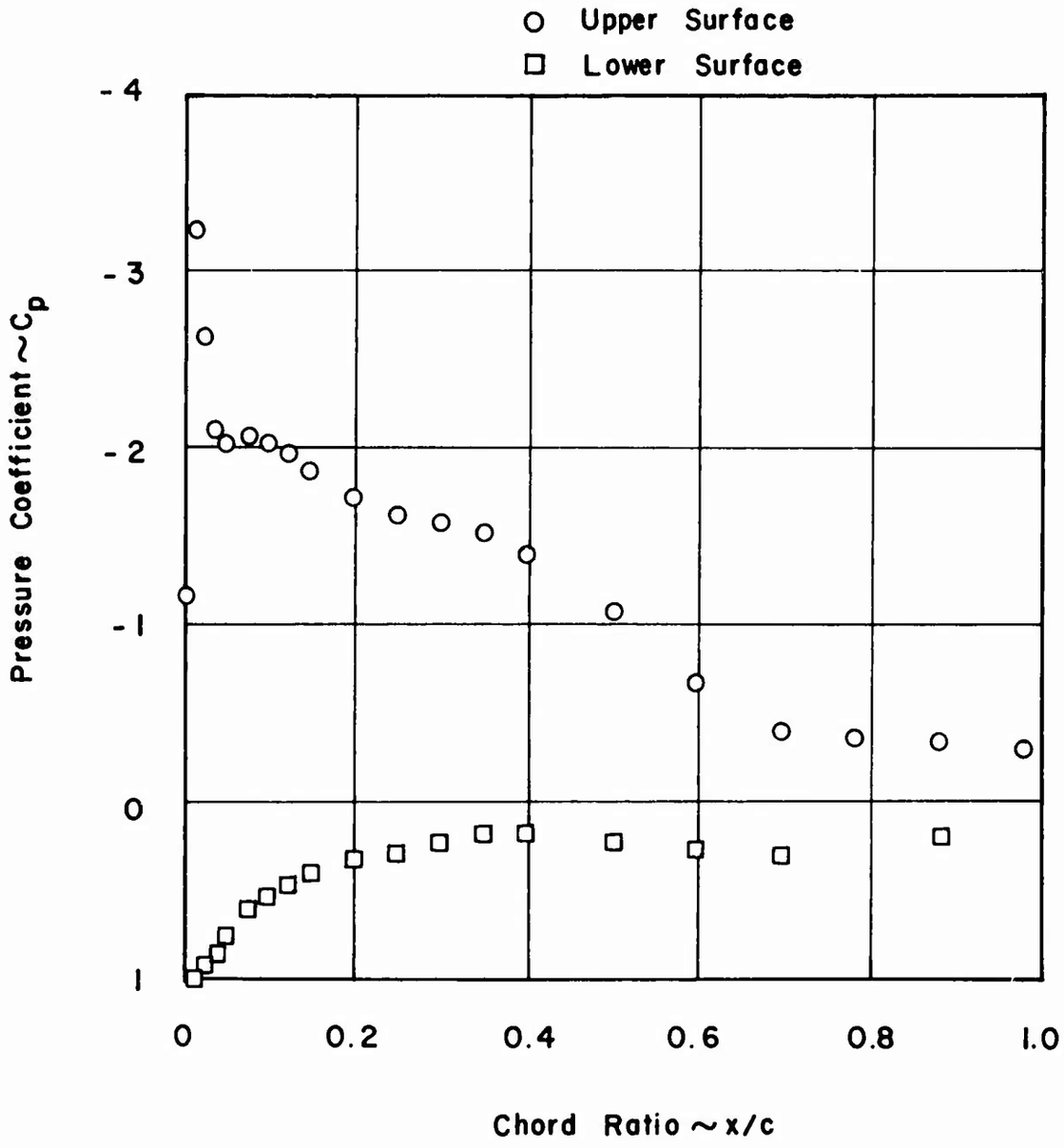

Figure 15. Pressure Distribution, Impervious Model, 10^{o} Camber, $\alpha = 8^{o}$.

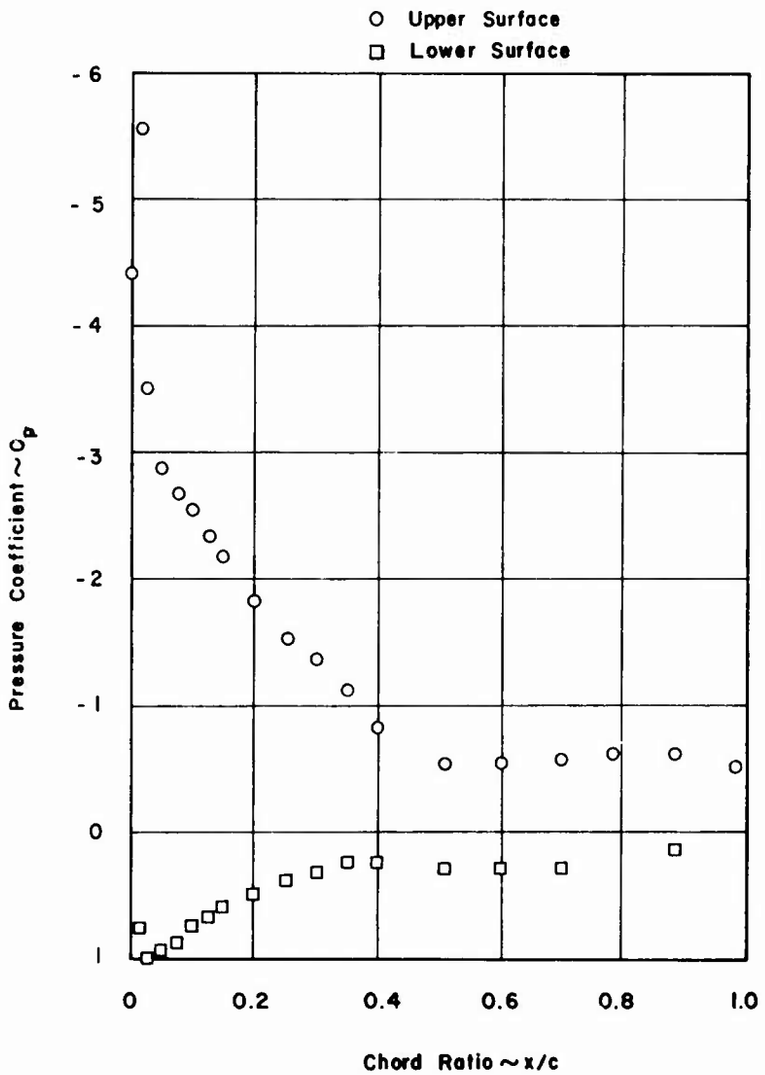

Figure 16. Pressure Distribution, Impervious Model, 10^{0} Camber, $\alpha = 16^{0}$.

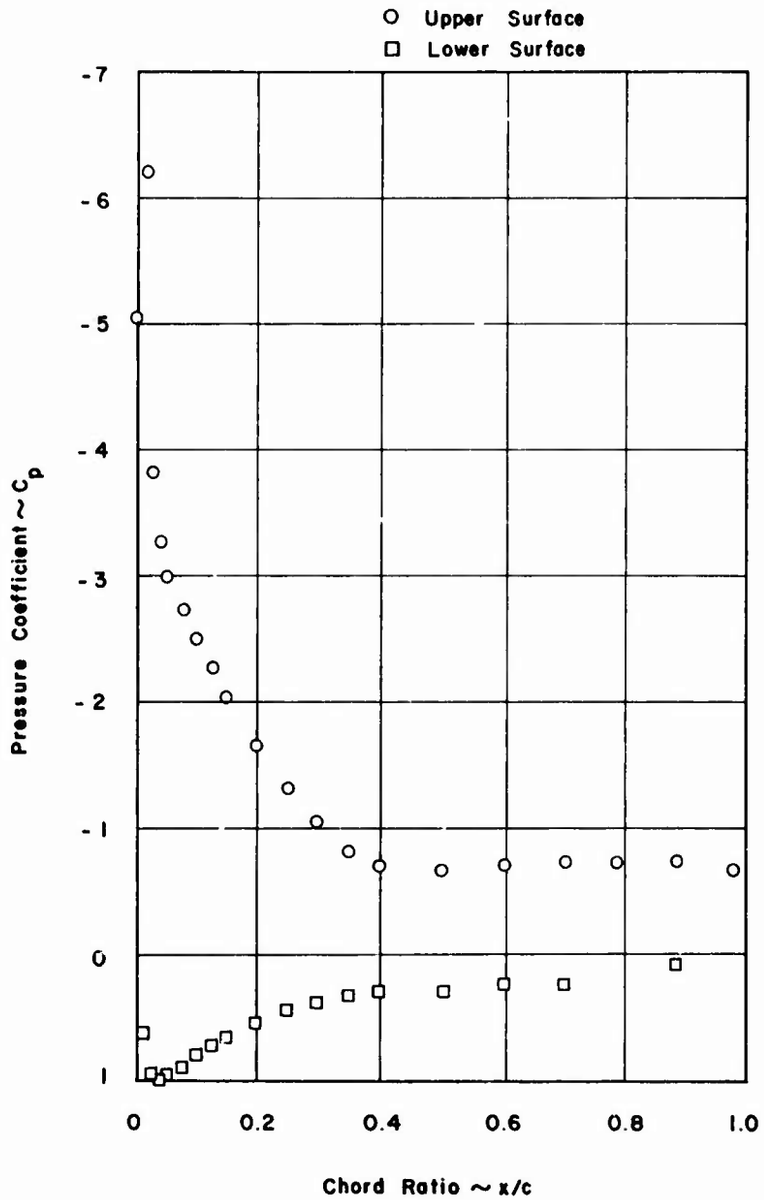

Figure 17. Pressure Distribution, Impervious Model, 10^{0} Camber, $\alpha = 18^{0}$.

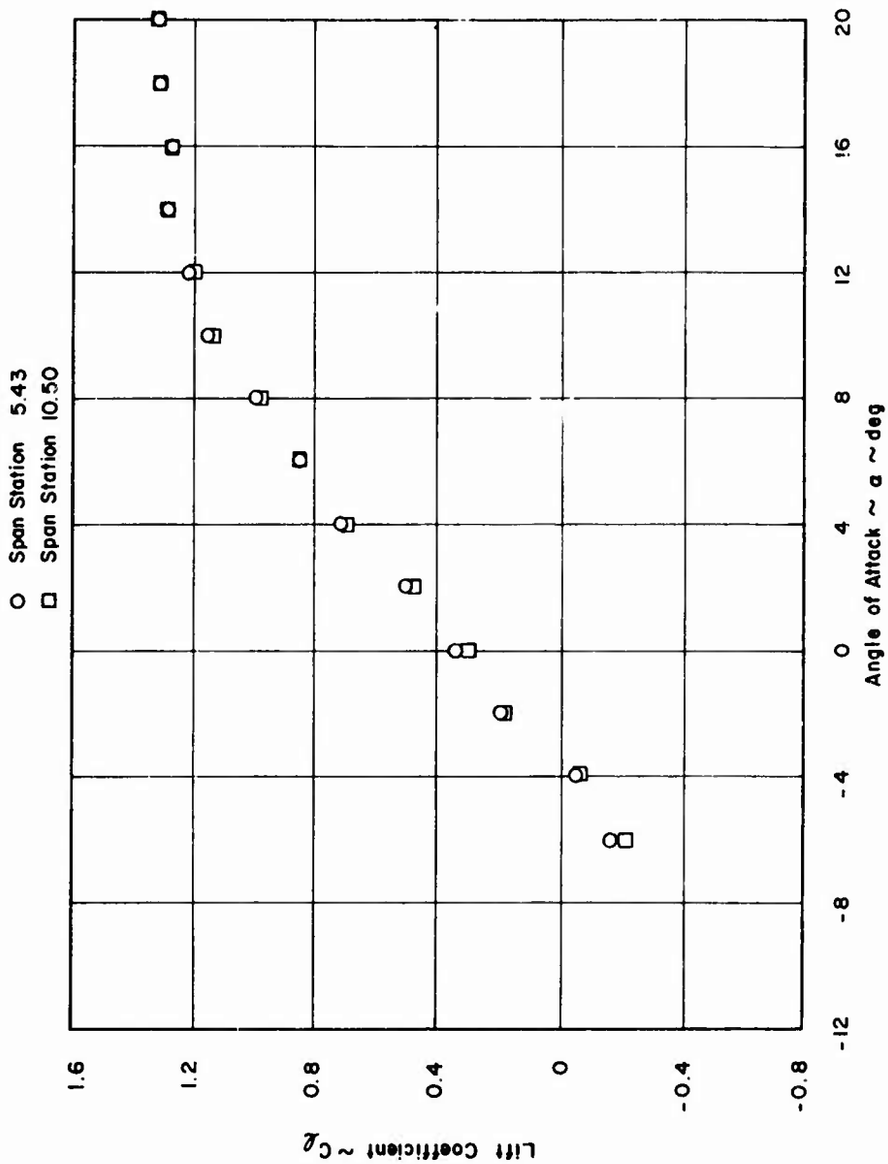

Figure 18. Lift Characteristics, Impervious Model, 0^{o} Camber, $R_N = 1.02 \times 10^6$.

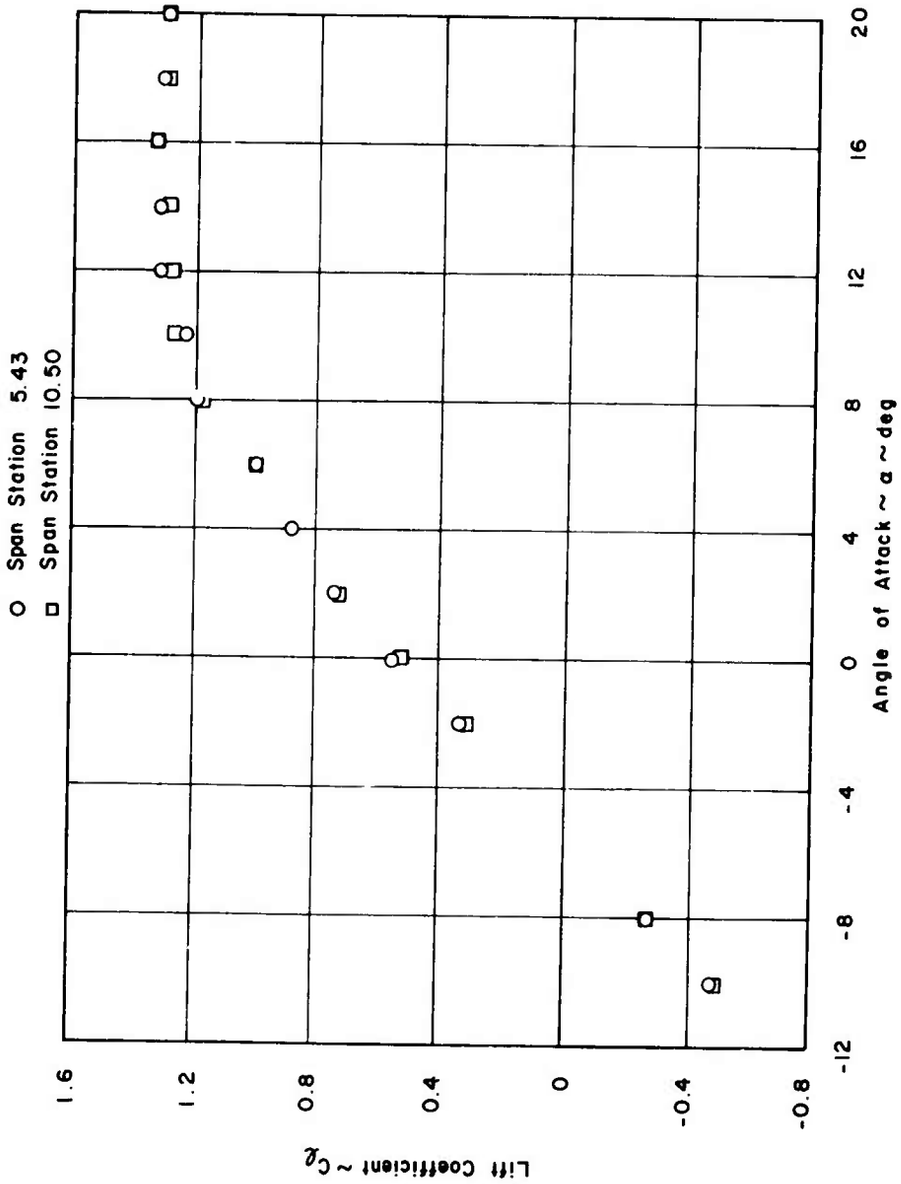

Figure 19. Lift Characteristics, Impervious Model, 5^0 Camber, $R_N = 1.02 \times 10^6$.

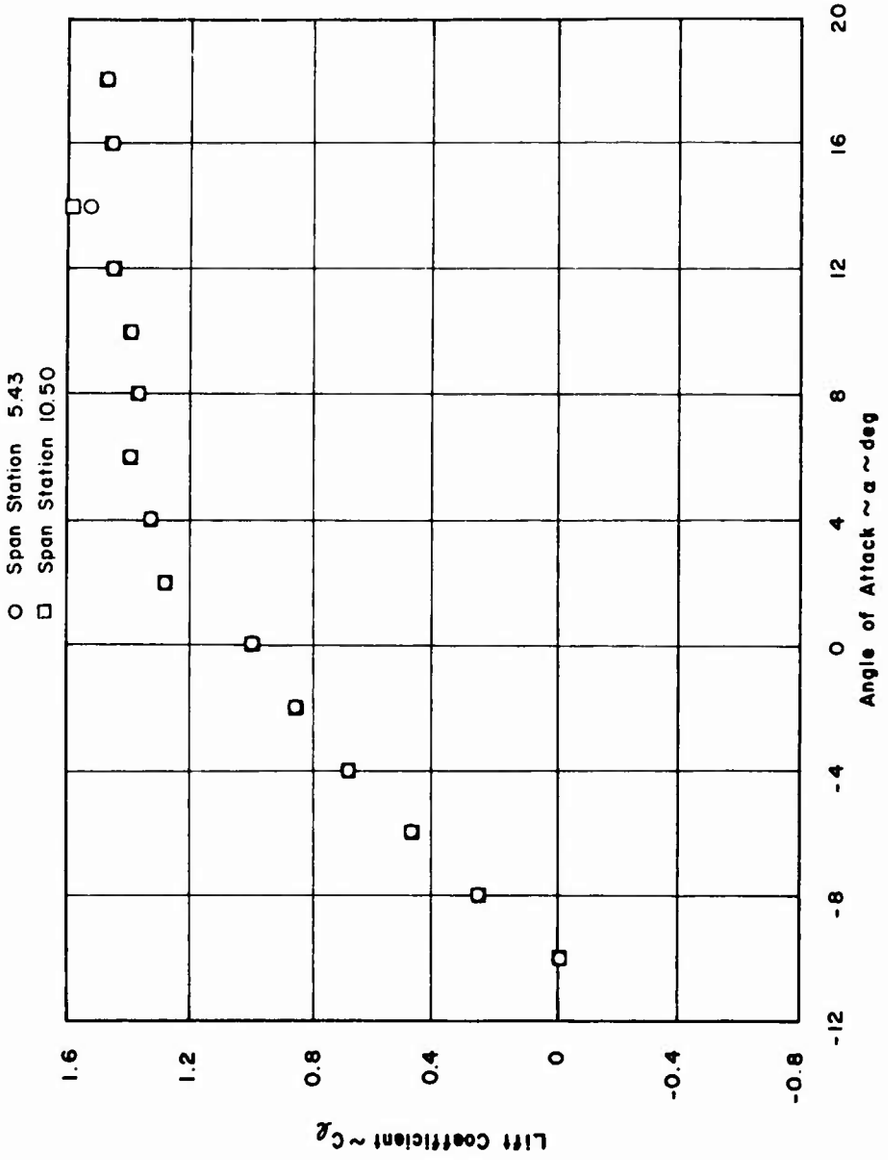

Figure 20. Lift Characteristics, Impervious Model, 10^0 Camber, $R_N = 1.02 \times 10^6$.

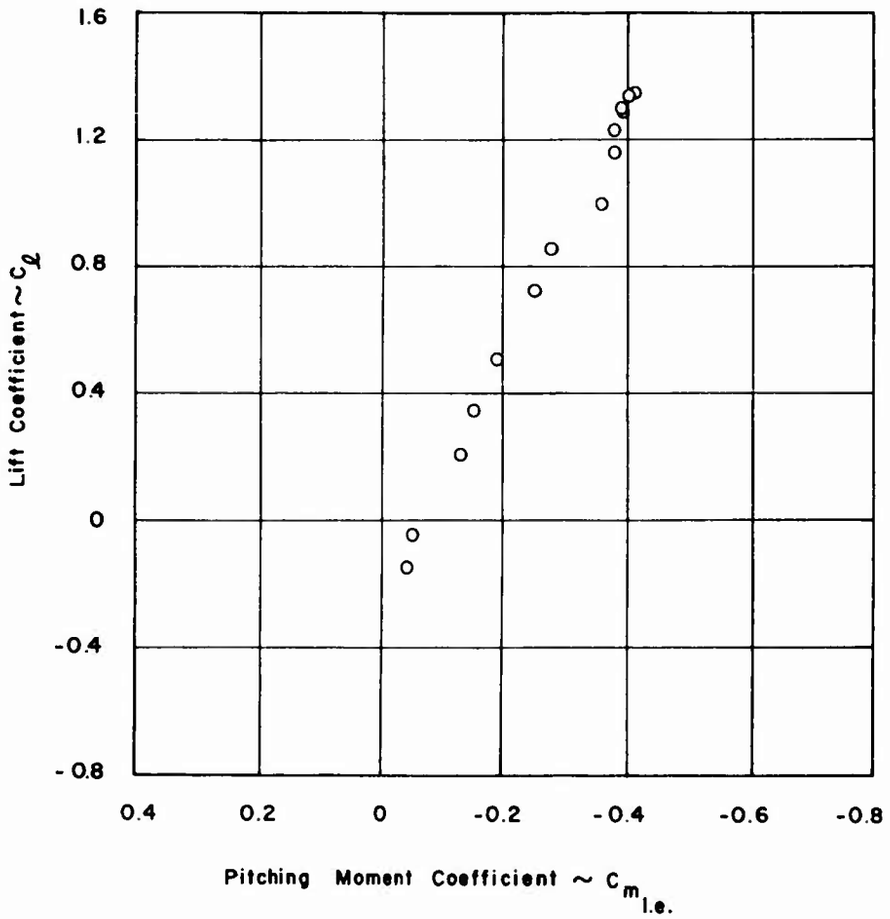

Figure 21. Pitching Moment Characteristics, Impervious Model, 0^{o} Camber, $R_N = 1.02 \times 10^6$.

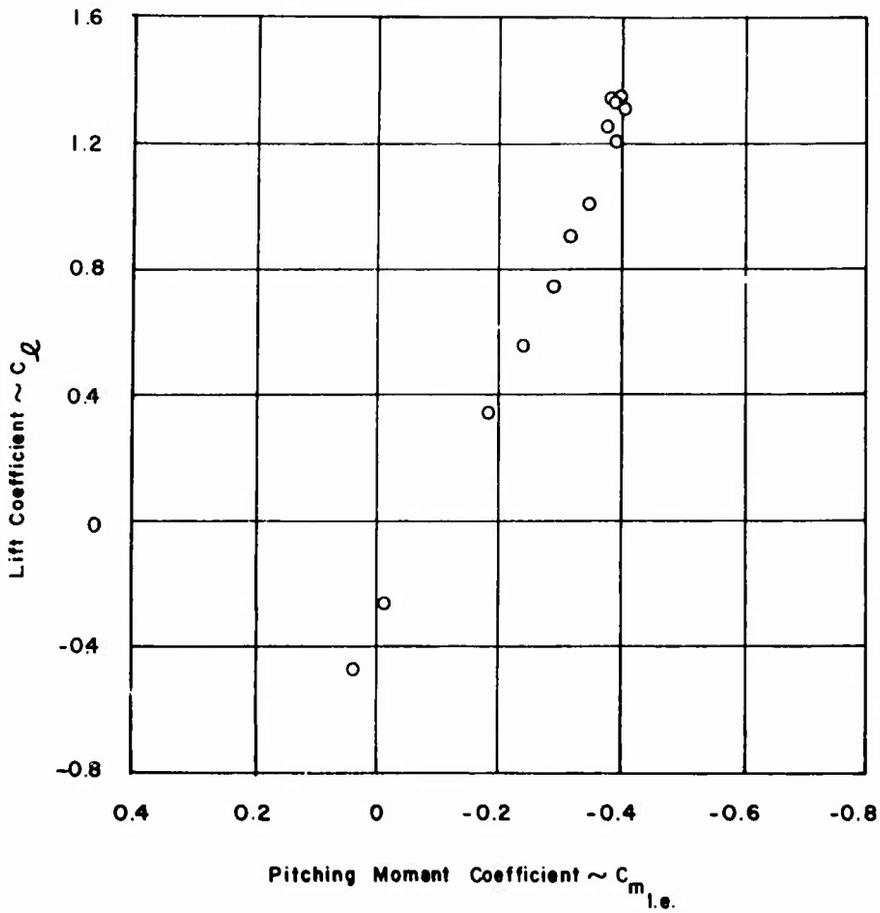

Figure 22. Pitching Moment Characteristics, Impervious Model, 5^0 Camber, $R_N = 1.02 \times 10^6$.

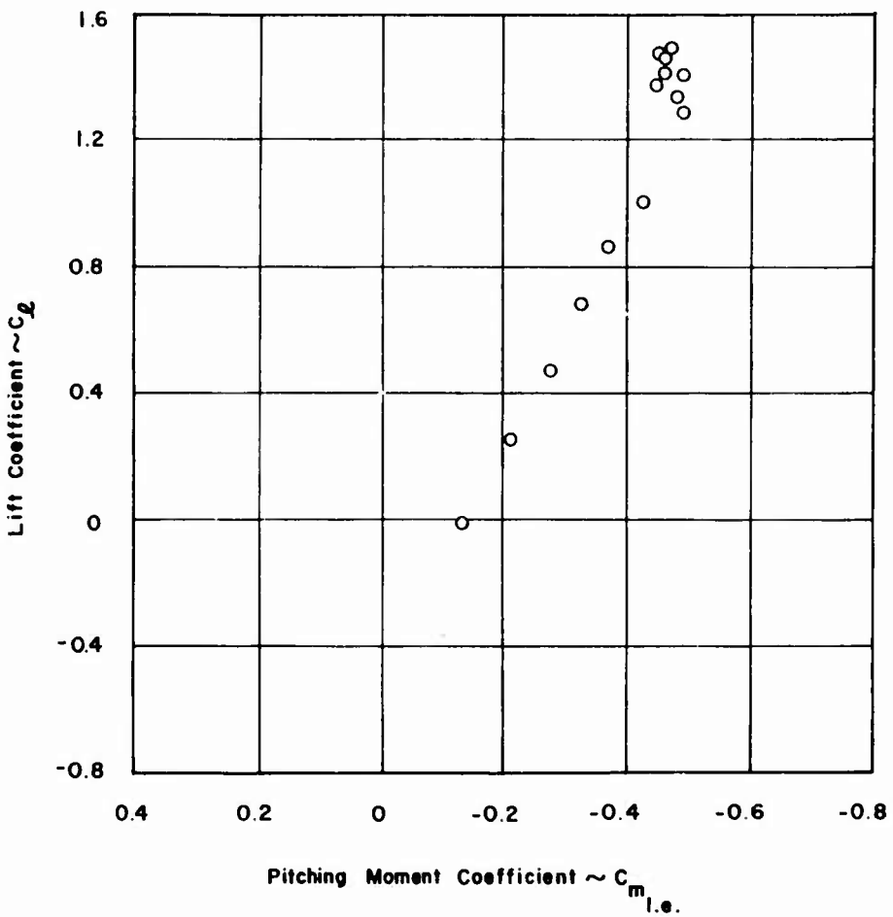

Figure 23. Pitching Moment Characteristics, Impervious Model, 10^{o} Camber, $R_N = 1.02 \times 10^6$.

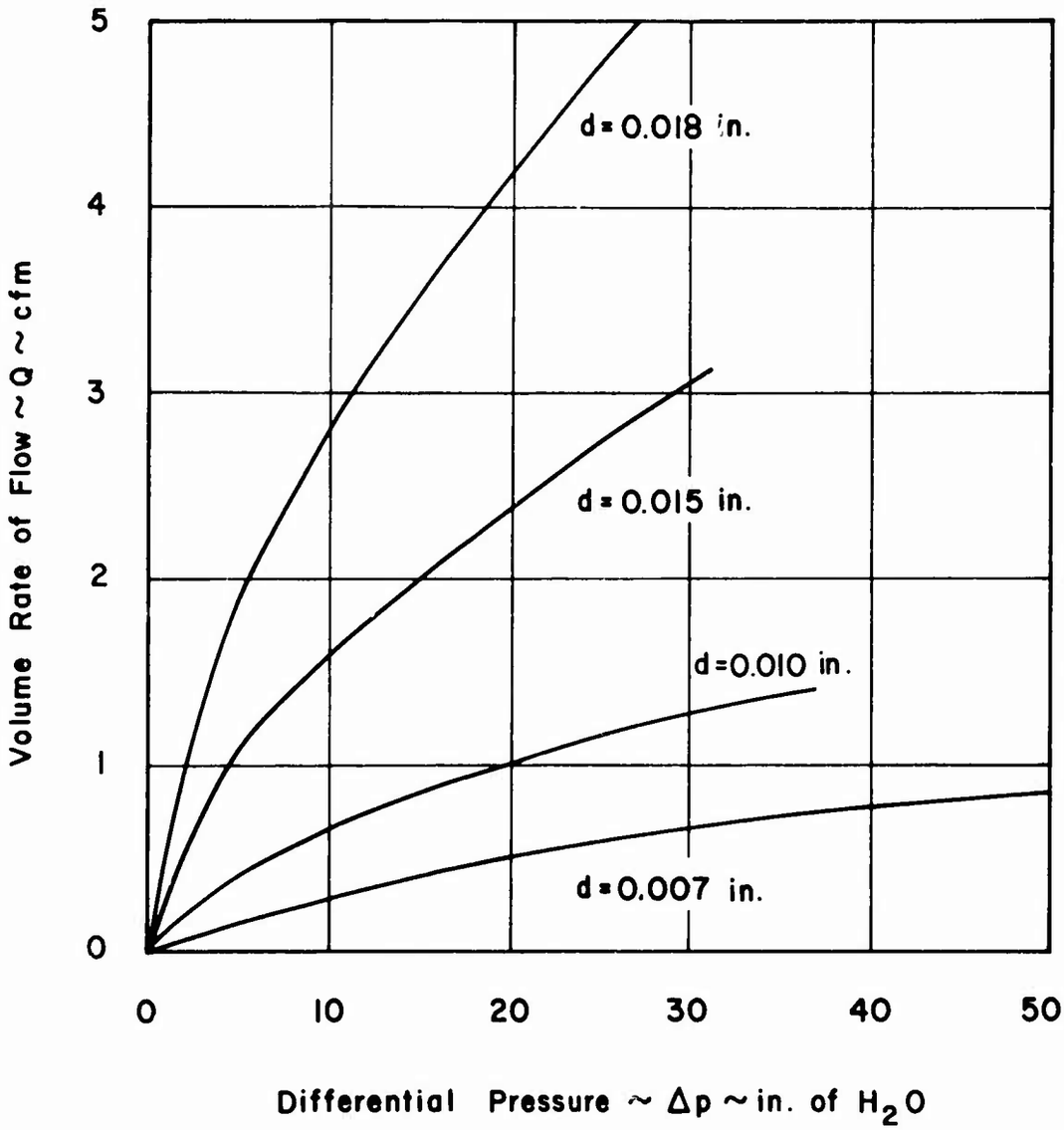

Figure 24. Porosity Data for 120 Suction Holes.

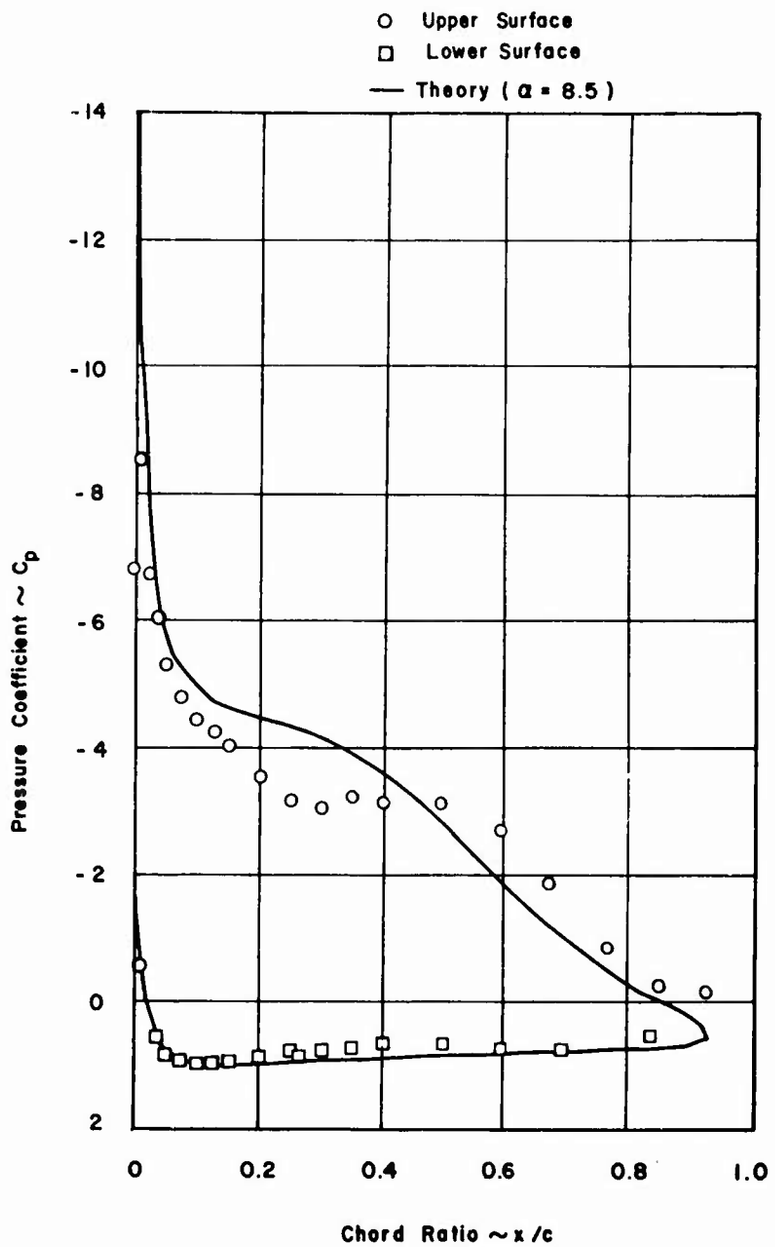

Figure 25. Pressure Distribution, Suction Model, 30^{o} Camber, $\alpha = 8^{o}$.

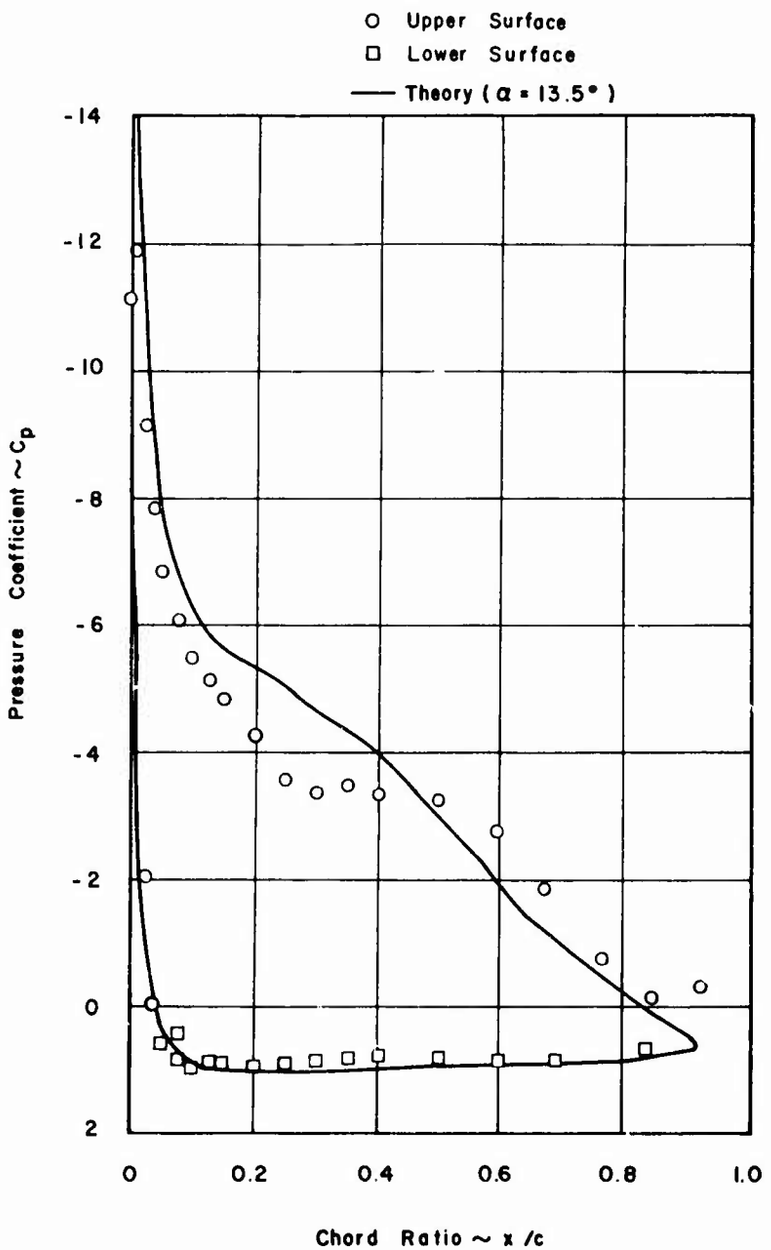

Figure 26. Pressure Distribution, Suction Model, 30^{o} Camber, $\alpha = 12^{o}$.

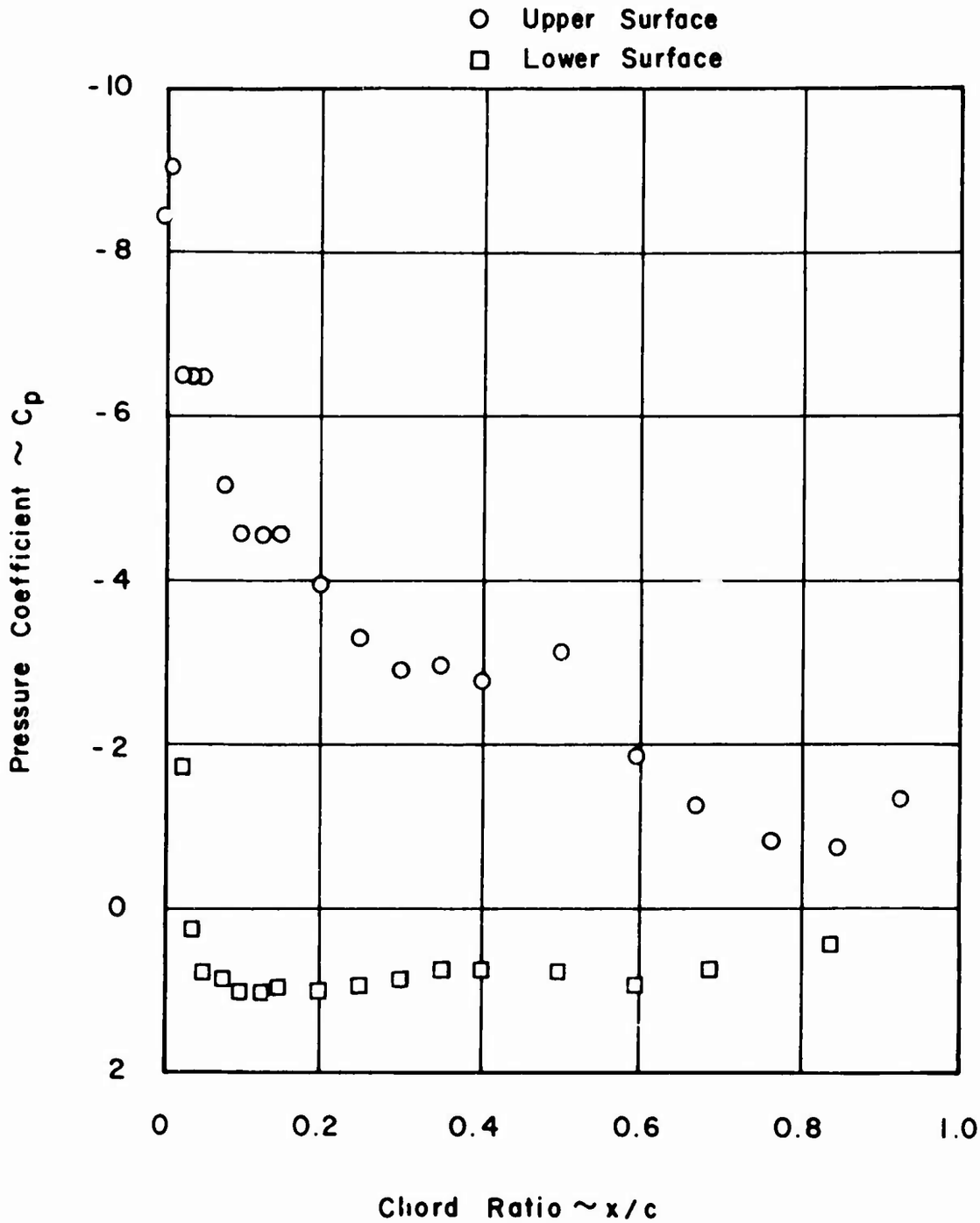

Figure 27. Pressure Distribution, Suction Model, 30^{o} Camber, $\alpha = 15^{o}$.

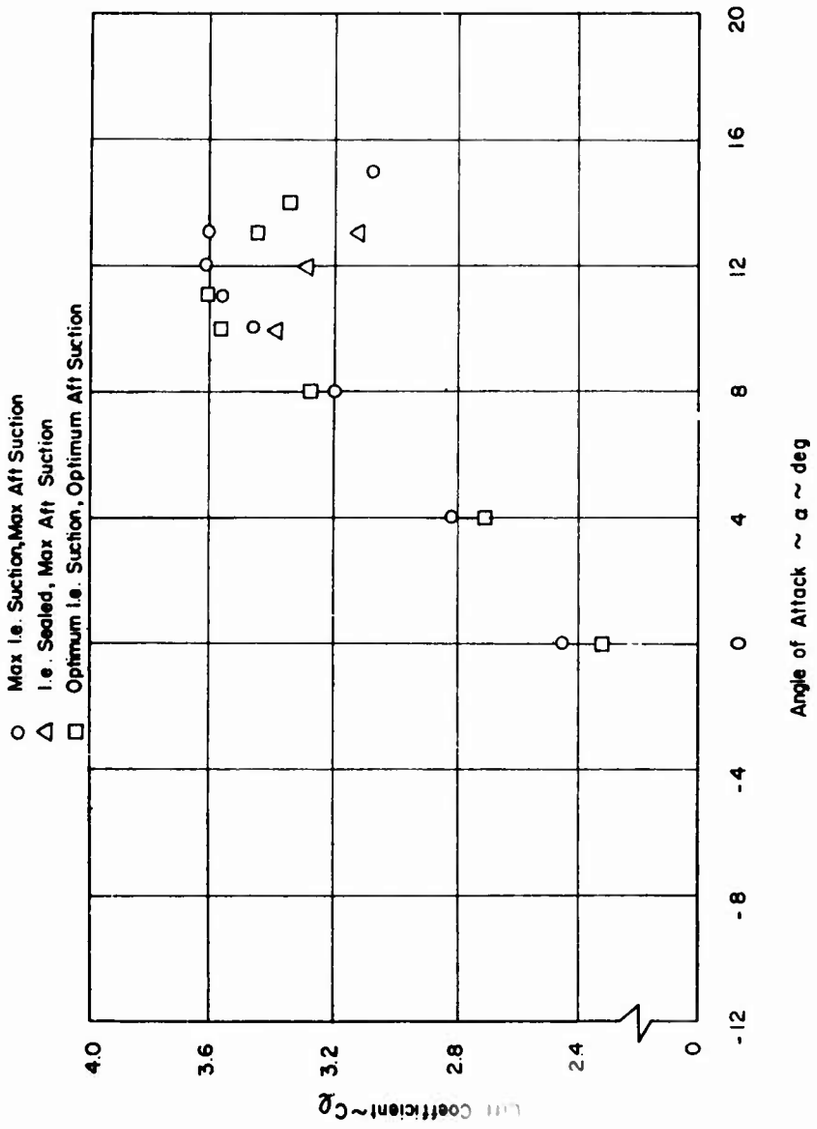

Figure 28. Lift Characteristics, Suction Model, 30^0 Camber, $R_N = 0.47 \times 10^6$.

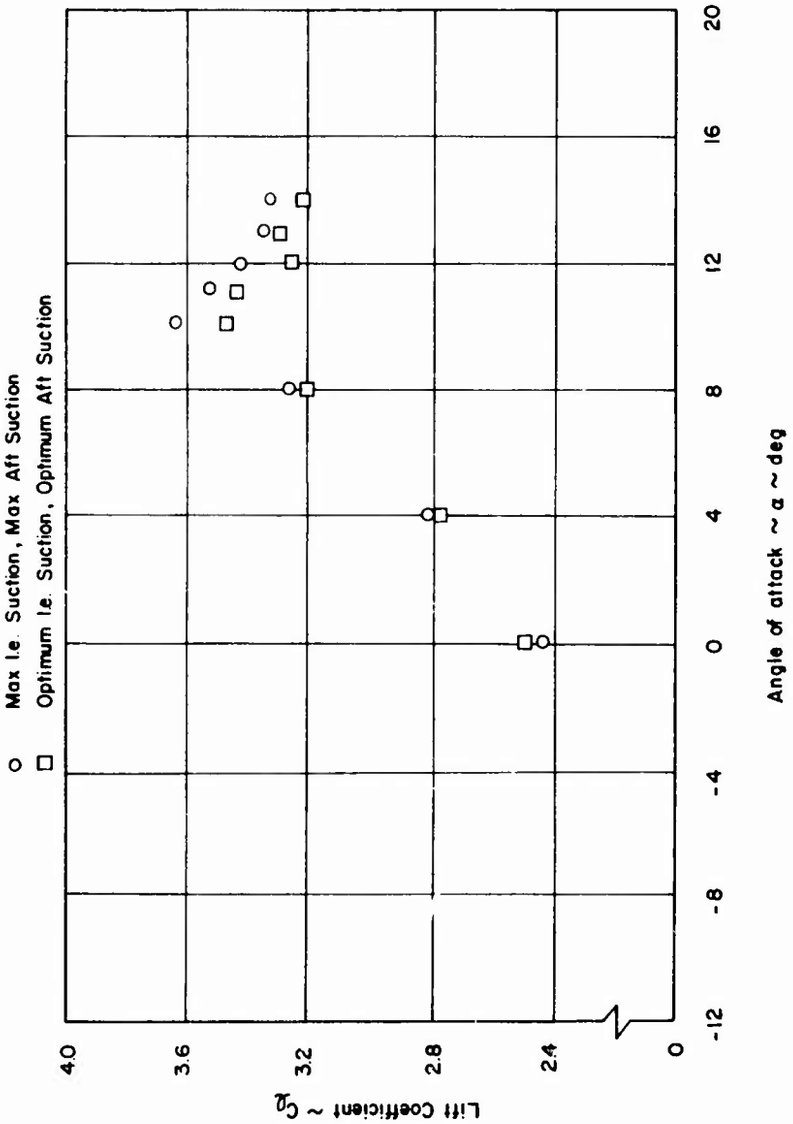

Figure 29. Lift Characteristics, Suction Model, 30^{0} Camber, $R_N = 0.64 \times 10^6$.

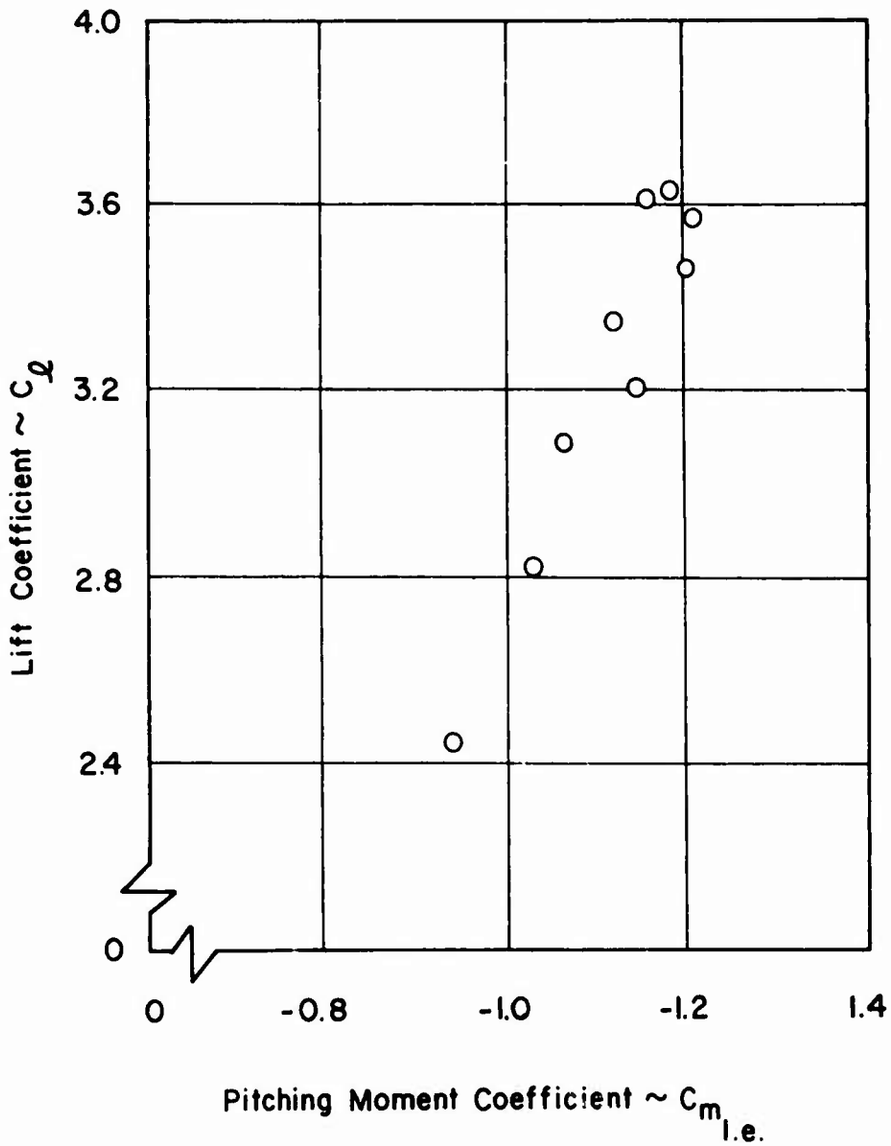

Figure 30. Pitching Moment Characteristics, Suction Model, Maximum l.e. and Aft Suction, 30^0 Camber, $R_N = 0.47 \times 10^6$.

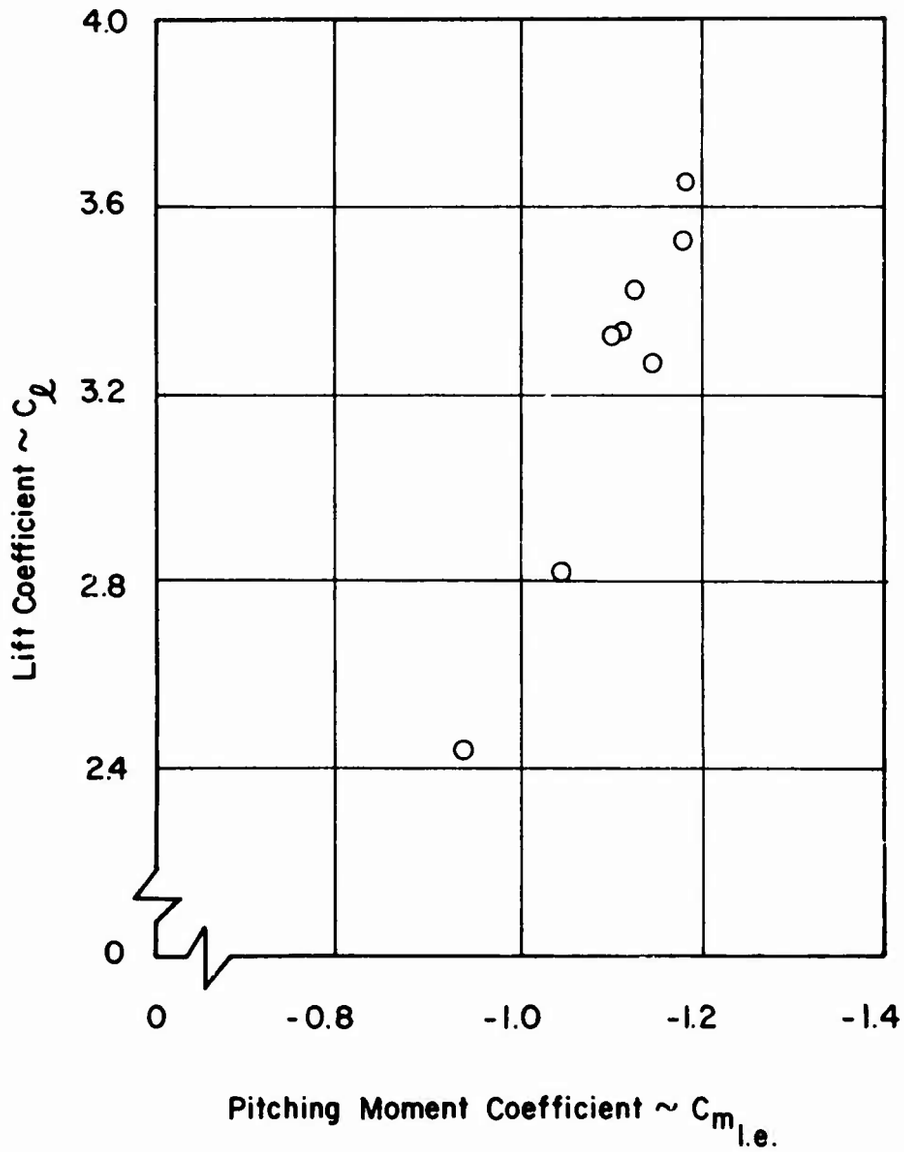

Figure 31. Pitching Moment Characteristics, Suction Model, Maximum l.e. and Aft Suction, 30° Camber, R_N = 0.64 x 10^6.

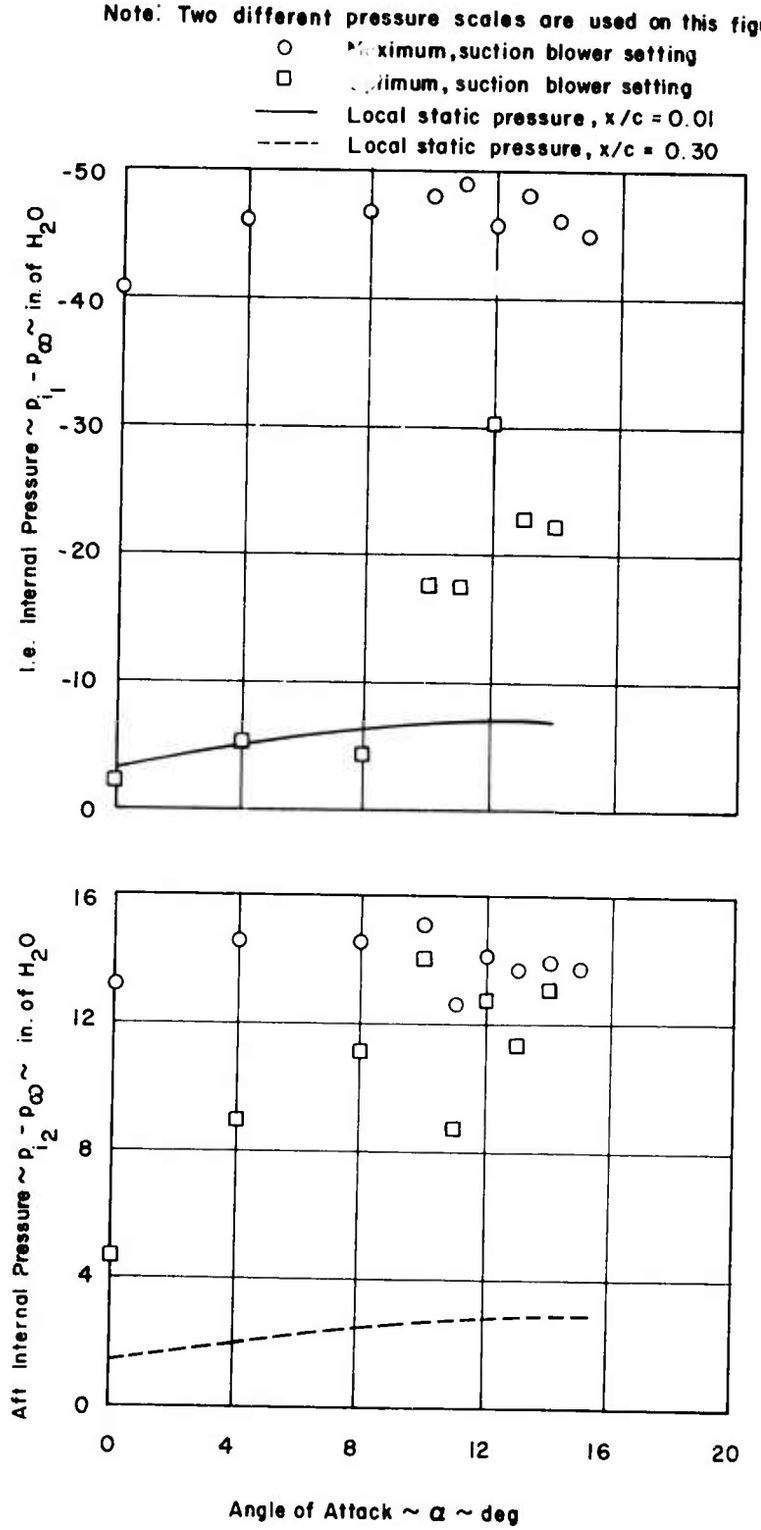

Figure 32. Internal Wing Suction Pressures Used in Test, Suction Model, 30^0 Camber, $R_N = 0.47 \times 10^6$.

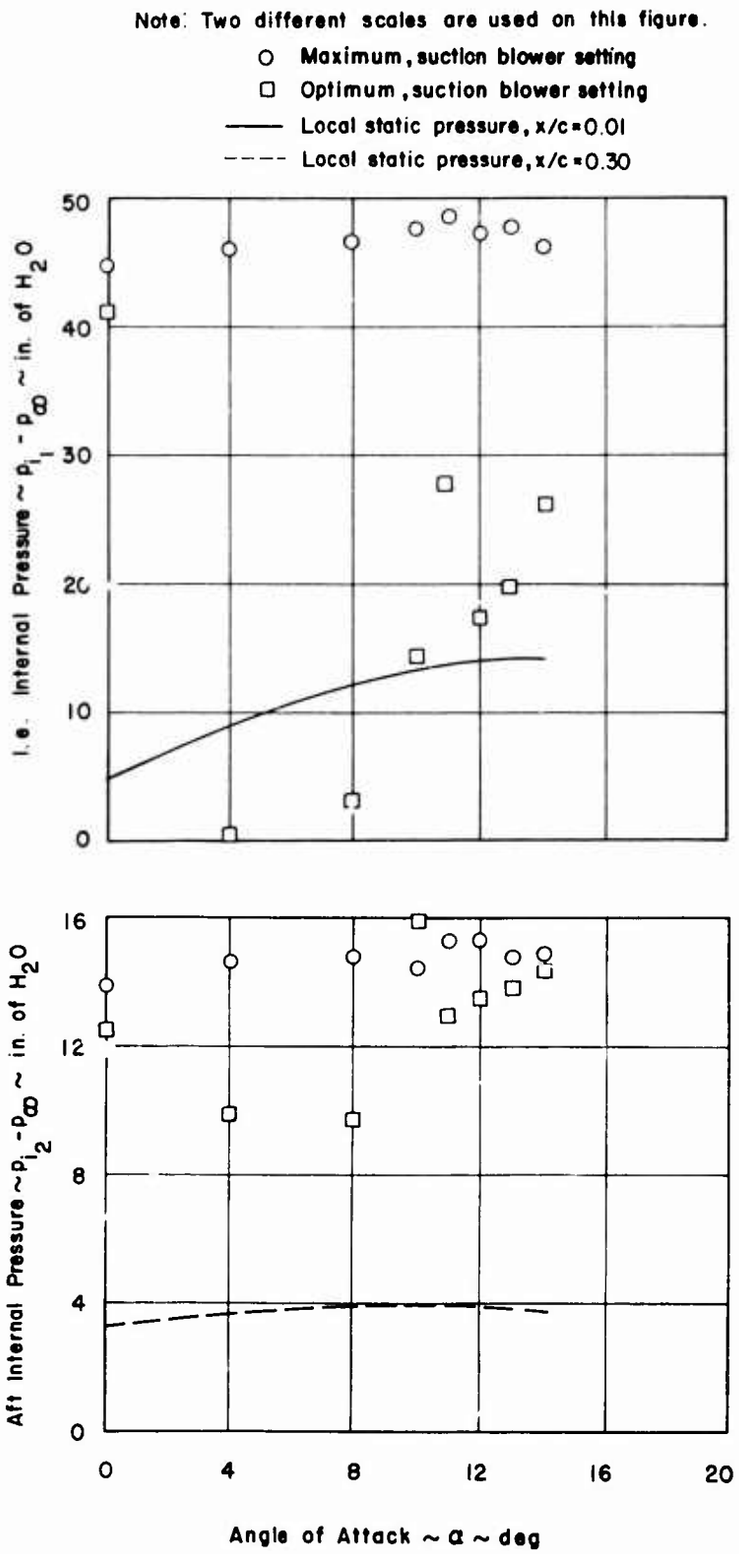

Figure 33. Internal Wing Suction Pressures Used in Test, Suction Model, 30^0 Camber, $R_N = 0.54 \times 10^6$.

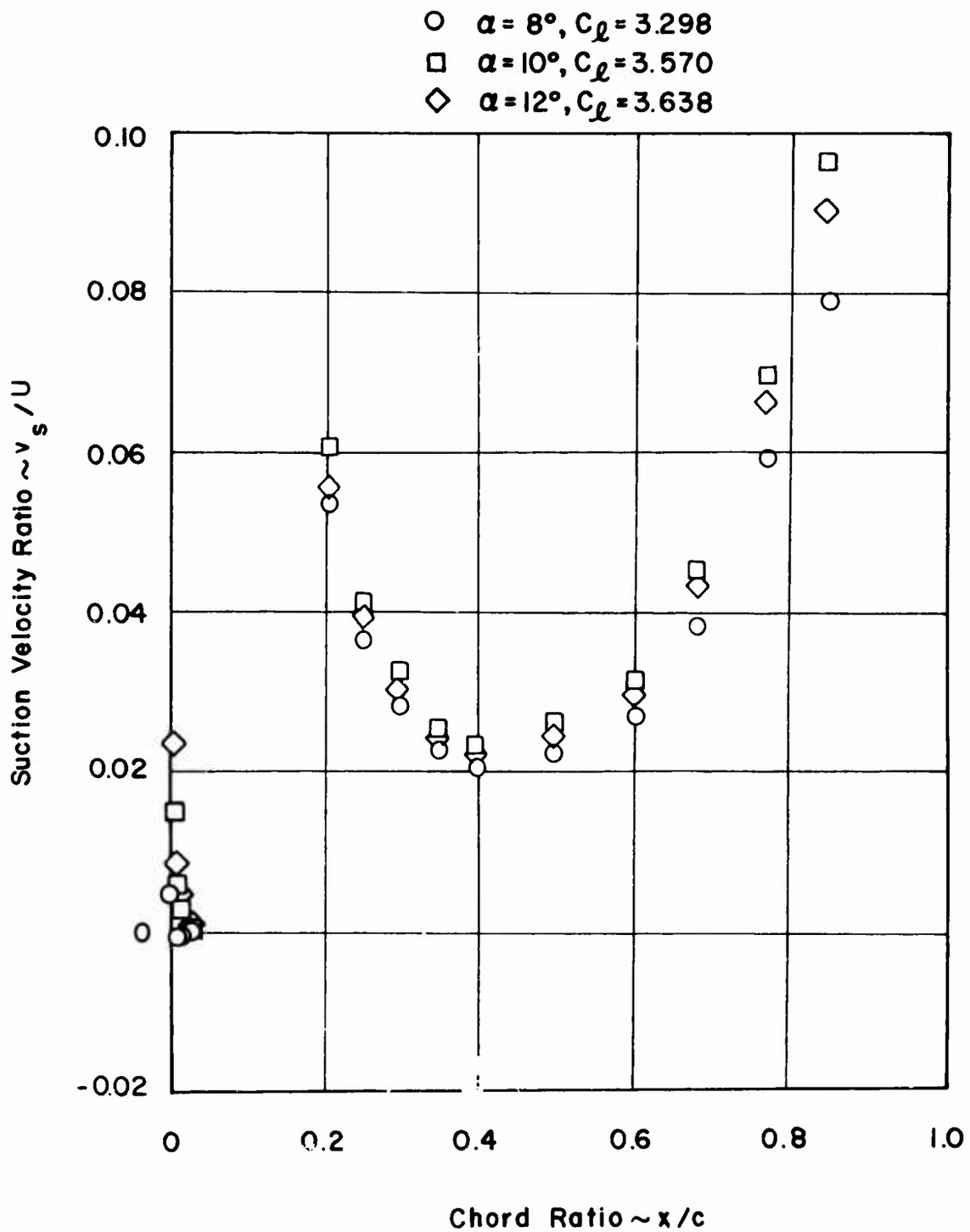

Figure 34. Optimum Suction Velocity Ratio Distribution, Suction Model, 30^0 Camber, $R_N = 0.47 \times 10^6$.

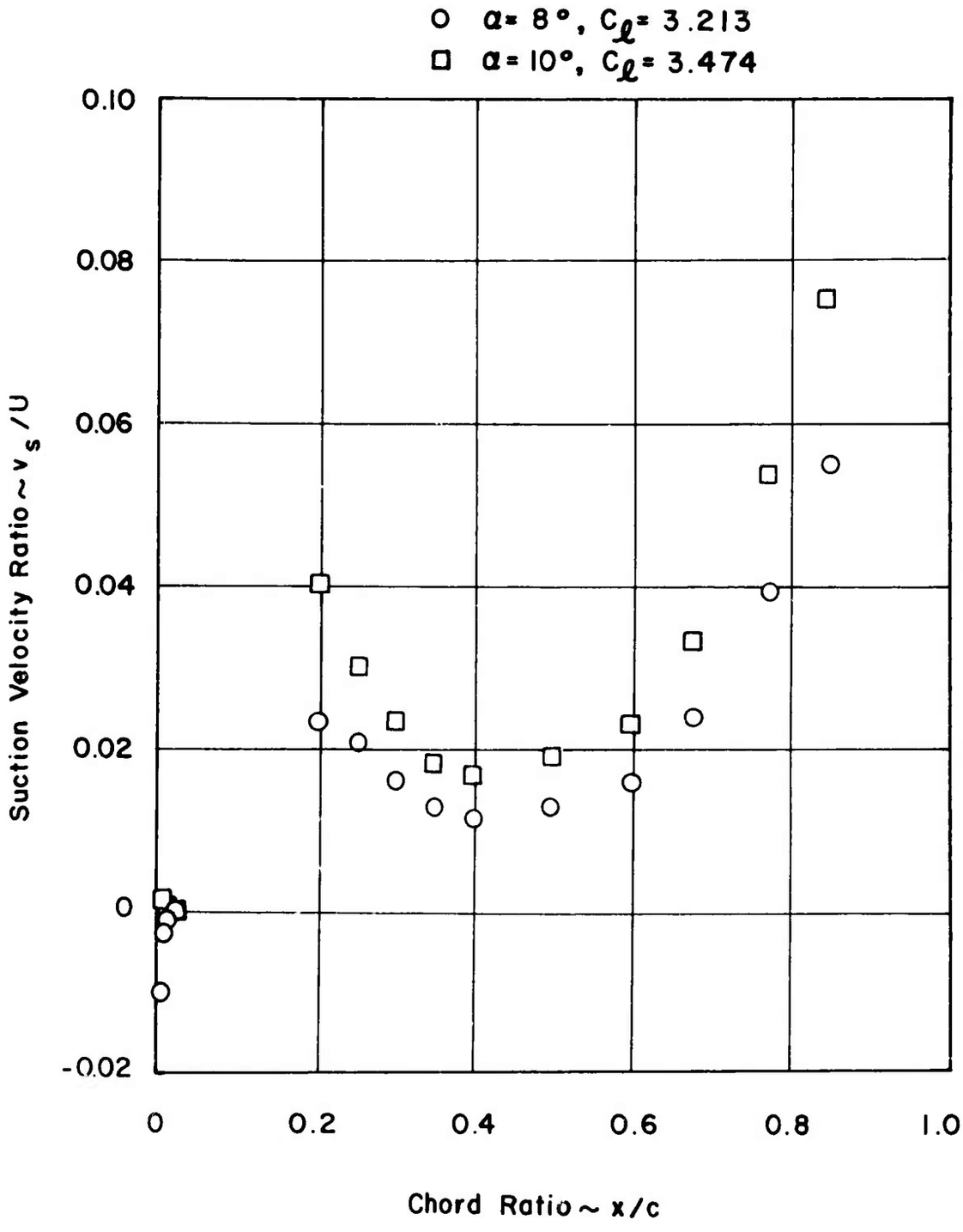

Figure 35. Optimum Suction Velocity Ratio Distribution, Suction Model, 30^0 Camber, R_N = 0.64 x 10^6.

LITERATURE CITED

1. Roberts, Seán C., Smith, Michael R., and Clark, David G., FLIGHT TEST EVALUATION OF A DISTRIBUTED SUCTION HIGH-LIFT BOUNDARY LAYER CONTROL SYSTEM ON A MODIFIED L-19 LIAISON AIRCRAFT, Mississippi State University, USAAVLABS Technical Report 66-36, U. S. Army Aviation Materiel Laboratories, Fort Eustis, Virginia, May 1966, AD 635 953.

2. Mertaugh, L. J., Roberts, S. C., and Kiran, N. S., XV-11A FLIGHT TEST PROGRAM, Mississippi State University, USAAVLABS Technical Report 70-37, Eustis Directorate, U. S. Army Air Mobility Research and Development Laboratory, Fort Eustis, Virginia, February 1971, AD 724 124.

3. Schlichting, Hermann (translated by Kestin, J.), BOUNDARY-LAYER THEORY, Sixth Edition, New York, McGraw-Hill Book Company, 1968, p. 711.

4. Pinkerton, Robert M., CALCULATED AND MEASURED PRESSURE DISTRIBUTIONS OVER THE MIDSPAN SECTION OF THE NACA 4412 AIRFOIL, NACA, Report Number 563, 1931.

5. Truckenbrodt, E., A METHOD OF QUADRATIVE FOR CALCULATION OF THE LAMINAR AND TURBULENT BOUNDARY-LAYER IN CASE OF PLANE AND ROTATIONALLY SYMMETRICAL FLOW, NACA, RM 1379, May 1955.

6. Thompson, Joe F., A FORTRAN PROGRAM OF THE TRUCKENBRODT LAMINAR AND TURBULENT BOUNDARY-LAYER CALCULATION, Mississippi State University, Aerophysics and Aerospace Engineering Department, Research Note Number 29, August 1967.

7. Wuest, W., EXPERIMENTAL INVESTIGATION ON BOUNDARY-LAYER SUCTION BY SERIES OF SLITS AND HOLES, Advisory Group for Aeronautical Research and Development, Report 258, April 1960.

8. Dodds, J. I., THE USE OF SUCTION OR BLOWING TO PREVENT SEPARATION OF A TURBULENT BOUNDARY-LAYER, Blackburn Aircraft Limited, Aerodynamics Department, Note Number YLP 1022, June 1961.

9. Ludwieg, H., and Tillmann, W., INVESTIGATIONS OF THE WALL-SHEARING STRESS IN TURBULENT BOUNDARY LAYERS, NACA, TM 1285, May 1950.

10. Eppler, R., PRAKTISHE BERECHNUNG LAMINARER AND TURBULENTER ABSAUGE-GREUZCHICHTEN, Ingenieur-Archiv, 32. Band 4, Heft, 1963, pp. 221-245.

11. Mertaugh, L. J., Burt, S., INVESTIGATION OF THE SUCTION SYSTEM AND BOUNDARY-LAYER CHARACTERISTICS ON A HIGH-LIFT, BLC L-19 TEST AIRCRAFT, Mississippi State University, USAAMRDL Technical Report 73-2, Eustis Directorate, U. S. Army Air Mobility Research and Development Laboratory, Fort Eustis, Virginia , May 1973.

12. Mertaugh, Lawrence J., FEASIBILITY STUDY OF A COMBINED LAMINAR AND TURBULENT BOUNDARY LAYER CONTROL SYSTEM USING DISTRIBUTED SUCTION, Mississippi State University, AFFDC-TR-71-47, Air Force Flight Dynamics Laboratory, Air Force Systems Command, Wright-Patterson Air Force Base, Ohio, April 1971, p. 32.

13. Abbott, Ira H., von Doeuhoff, Albert E., and Stives, Louis S., Jr., SUMMARY OF AIRFOIL DATA, NACA, Report Number 824, 1945, p. 169.

14. Ward, G. F., MEASUREMENT OF THE FLOW THROUGH SMALL HOLES, Aerodynamics Note 127, Department of Supply, Research and Development Branch, Aeronautical Research Laboratories, Commonwealth of Australia, September 1953.